





# The small molecule GAT1508 activates brain-specific GIRK1/2 channel heteromers and facilitates conditioned fear extinction in rodents

Received for publication, October 18, 2019, and in revised form, January 9, 2020. Published, Papers in Press, January 17, 2020, DOI 10.1074/jbc.RA119.011527

Yu Xu<sup>†1</sup>, Lucas Cantwell<sup>†1</sup>,  Andrei I. Molosh<sup>§</sup>,  Leigh D. Plant<sup>‡</sup>, Dimitris Gazgalis<sup>‡</sup>, Stephanie D. Fitz<sup>§</sup>, Erik T. Dustrude<sup>§</sup>, Yuchen Yang<sup>‡</sup>, Takeharu Kawano<sup>‡</sup>, Sumanta Garai<sup>‡</sup>, Sami F. Noujaim<sup>¶</sup>, Anantha Shekhar<sup>§2</sup>, Diomedes E. Logothetis<sup>‡3</sup>, and Ganesh A. Thakur<sup>‡4</sup>

From the <sup>†</sup>Department of Pharmaceutical Sciences, School of Pharmacy, Bouvé College of Health Sciences, and Center for Drug Discovery, Northeastern University, Boston, Massachusetts 02115, the <sup>§</sup>Department of Psychiatry, Paul and Carole Stark Neurosciences Research Institute, Indiana Clinical and Translational Sciences Institute, Indiana University School of Medicine, Indianapolis, Indiana 46202, and the <sup>¶</sup>Molecular Pharmacology and Physiology, University of South Florida, Tampa, Florida 33612

Edited by Henrik G. Dohlman

G-protein–gated inwardly-rectifying K<sup>+</sup> (GIRK) channels are targets of G<sub>i/o</sub>-protein–signaling systems that inhibit cell excitability. GIRK channels exist as homotetramers (GIRK2 and GIRK4) or heterotetramers with nonfunctional homomeric subunits (GIRK1 and GIRK3). Although they have been implicated in multiple conditions, the lack of selective GIRK drugs that discriminate among the different GIRK channel subtypes has hampered investigations into their precise physiological relevance and therapeutic potential. Here, we report on a highly-specific, potent, and efficacious activator of brain GIRK1/2 channels. Using a chemical screen and electrophysiological assays, we found that this activator, the bromothiophene-substituted small molecule GAT1508, is specific for brain-expressed GIRK1/2 channels rather than for cardiac GIRK1/4 channels. Computational models predicted a GAT1508-binding site validated by experimental mutagenesis experiments, providing insights into how urea-based compounds engage distant GIRK1 residues required for channel activation. Furthermore, we provide computational and experimental evidence that GAT1508 is an allosteric modulator of channel–phosphatidylinositol 4,5-bisphosphate interactions. Through brain-slice electrophysiology, we show that subthreshold GAT1508 concentrations directly stimulate GIRK currents in the basolateral amygdala (BLA) and potentiate baclofen-induced currents. Of note, GAT1508 effectively extinguished conditioned fear in rodents and lacked cardiac and behavioral side effects, suggesting its potential for use in pharmacotherapy for post-traumatic stress disorder. In summary, our findings indicate that the small mole-

cule GAT1508 has high specificity for brain GIRK1/2 channel subunits, directly or allosterically activates GIRK1/2 channels in the BLA, and facilitates fear extinction in a rodent model.

G-protein–gated inwardly-rectifying potassium (K<sup>+</sup>) (GIRK<sup>5</sup> or Kir3) channels are activated by G<sub>i/o</sub>-dependent (pertussis toxin-sensitive) signaling pathways in the heart and nervous system (1–6). Their activation inhibits excitability, slowing the rate of pacemaker and atrial cell firing in the heart, inhibiting transmitter release by pre-synaptic neurons, or opposing excitation of post-synaptic neurons. Polymorphisms and mutations in human GIRK channels have been linked to arrhythmias, hyperaldosteronism (and associated hypertension), sensitivity to analgesics, addiction, alcohol dependence, anxiety, and schizophrenia (7–10). GIRK channels are activated by binding of the G-protein βγ (Gβγ) subunits (1, 3–7, 11–13). Gβγ binding strengthens channel affinity for phosphatidylinositol 4,5-bisphosphate (PIP<sub>2</sub>), a necessary cofactor for channel gating (14–17). Structural studies, using crystallography or computational modeling, have produced three-dimensional models of the interactions of GIRK channels with PIP<sub>2</sub> and the Gβγ subunits (16, 18–20). GIRK channels are also activated in a G-protein–independent manner by intracellular Na<sup>+</sup> (21–24), ethanol (25, 26), volatile anesthetics (27, 28), and naringin (29), again in a PIP<sub>2</sub>-dependent manner (15). Many psychoactive and

This work was supported by National Institutes of Health Grants R01-EY024717 (to G. A. T.), R01-HL059949-21 and R01-HL059949-22 (to D. E. L.), and R01-MH052619, R01-MH065702, UL1-TR001108 (to A. S.), R21-HL138064, and R01-HL129136 (to S.F.N.). The authors declare that they have no conflicts of interest with the contents of this article. The content is solely the responsibility of the authors and does not necessarily represent the official views of the National Institutes of Health.

This article contains Figs. S1–S10 and supporting Chemistry.

<sup>1</sup> Both authors contributed equally to this work.

<sup>2</sup> To whom correspondence may be addressed. E-mail: [ashekhar@iu.edu](mailto:ashekhar@iu.edu).

<sup>3</sup> To whom correspondence may be addressed. E-mail: [d.logothetis@northeastern.edu](mailto:d.logothetis@northeastern.edu).

<sup>4</sup> To whom correspondence may be addressed. E-mail: [g.thakur@northeastern.edu](mailto:g.thakur@northeastern.edu).

<sup>5</sup> The abbreviations used are: GIRK, G-protein–gated inwardly-rectifying K<sup>+</sup>; BLA, basolateral amygdala; SAR, structure-activity relationship; MD, molecular dynamics; HBC, helix bundle crossing; PCA, principal component analysis; CNS, central nervous system; APD, action potential duration; PAM, positive allosteric modulator; OF, open field; EPM, elevated plus maze; NOR, novel object recognition; TEVC, two-electrode voltage clamp; diC8, dioctanoyl; PIP<sub>2</sub>, phosphatidylinositol 4,5-bisphosphate; ANOVA, analysis of variance; OCRL, oculocerebrorenal syndrome protein; 5-ptase<sub>OCRL</sub>, 5' phosphatase domain from OCRL; CRY2, photolyase domain of cryptochrome 2; CIBN, CRY2-binding domain; ACSF, artificial cerebrospinal fluid solution; HR, heart rate; MAP, mean arterial blood pressure; SI, social interaction; MΩ, megohm; PDB, Protein Data Bank; POPC, 1-palmitoyl-2-oleoyl-L-phosphatidylcholine; POPE, 1-palmitoyl-2-oleoyl-*sn*-glycerol-3-phosphoethanolamine; POPS, 1-palmitoyl-2-oleoyl-*sn*-glycerol-3-phosphoserine; CS, conditioned stimulus; hERG, human ether-a-go-go-related gene; RM, repeated measures.

clinically relevant compounds with other primary molecular targets inhibit GIRK channels, albeit at relatively high doses (7, 30). GIRK channels are homo- and heterotetramers formed between the nonfunctional GIRK1 or GIRK3 with the functional GIRK2 and GIRK4 subunits (4, 6, 31–33). GIRK subunits exhibit overlapping but distinct cellular expression patterns, potentially yielding multiple channel subtypes (7, 31). Although it cannot form functional homotetramers (34–36), GIRK1 is an integral subunit of the cardiac GIRK channel and most neuronal GIRK channels (30, 33, 37). GIRK1 confers robust basal and receptor-dependent activity to GIRK heteromers, attributable in part to unique residues in the pore and second transmembrane domain (38–40). The intracellular C-terminal domain also contributes to the potentiating influence of GIRK1 on channel activity (41), likely due to the presence of unique structures that modify the interaction between the channel and  $G\beta\gamma$ ,  $G\alpha$ , and  $PIP_2$  (1, 4, 6, 7, 42). The lack of selective GIRK channel modulators, and in particular the ligands that discriminate among GIRK channel subtypes, has hampered investigation into their physiological relevance and therapeutic potential.

Recently, a class of small molecule GIRK channel activators with ML297 as the prototype has been shown to be a potent activator selective for GIRK1-containing channels (43–47). ML297 activates GIRK1-containing channels requiring only two amino acids specific to GIRK1, Phe-137 and Asp-173 (47). Although ML297 was shown to be more biased toward GIRK1/GIRK2 (or GIRK1/2) than GIRK1/GIRK4 (or GIRK1/4) heteromer activation, the significant activation of GIRK1/4 that is highly expressed in supraventricular cardiac tissues limits its utility as a potential drug-targeting GIRK1 heteromers expressed in the brain. Based on detailed *in vivo* studies of the pharmacological properties of the nonselective GIRK activators (44), it is evident that compounds that are fully selective for GIRK1/2 activation might represent a novel class of anxiolytic compounds with limited sedative and addictive liabilities. Here, we (a) report on a novel bromothiophene-substituted derivative, GAT1508, that achieves the desired full specificity for GIRK1/2 over GIRK1/4 subunits; (b) we elucidate the molecular basis for the specific mechanism of action of GAT1508; (c) we show its effectiveness as a direct or allosteric activator of GIRK1/2 channels in the basolateral amygdala (BLA) and (d) its efficacy in facilitating fear extinction in a rodent-conditioned fear paradigm that is utilized as a preclinical model of post-traumatic stress disorder.

## Results

### Chemical optimization and screening for specific GIRK1/2 over GIRK1/4 activation

Our first aim was to develop novel molecules that would be selective modulators of GIRK1/2 over GIRK1/4 channels. Initial chemical optimization focusing on Site I (R or difluorinated phenyl ring in ML297) resulted in 38 new analogs that were produced by a number of structure-activity relationship (SAR) strategies, such as spacer addition, heteroatom introduction, bioisosteric replacement, etc. (Fig. S1A and Fig. 1A). To explore the selectivity of these compounds, we evaluated their effects using two-electrode voltage-clamp of *Xenopus laevis* oocytes

expressing either brain or cardiac heteromeric GIRK channel subunits (brain GIRK1/2 versus cardiac GIRK1/4). Current responses to perfusion of 10  $\mu\text{M}$  of each compound were assessed (Fig. S1B summarizes current increases normalized to the basal current level in high potassium (HK) solution (*brown dashed line*) versus current level in compound tested relative to that of the ML297 compound (*purple dashed line*)). Similar to ML297, most compounds elicited greater current increases in GIRK1/2 compared with GIRK1/4 channels. Among them, two thiophene ring derivatives, one with a bromine and the other with a methyl at the 5' position, named GAT1508 and GAT1521, respectively, were the most selective GIRK1/2 activators relative to GIRK1/4 (Fig. S1B). Concentration-response curves of these two compounds compared with ML297, using whole-cell patch-clamp electrophysiology in HEK293 cells expressing GIRK1/2 or GIRK1/4 channels (Fig. 1B), further confirmed the selectivity for activation of the brain-expressing subunits and determined that GAT1508 possessed the highest potency and efficacy compared with ML297 or GAT1521.

Further structure-activity relationships were pursued in *Xenopus* oocytes. The thiophene ring with no substituents (GAT1506, Fig. S2B) lacked selectivity and was less potent than GAT1508. We then tested different halogens in order of varying size instead of bromine at position 5' of the thiophene ring. A fluorine-substituted thiophene, which occupies a smaller volume than bromine (GAT1575, Fig. S2C), was highly efficacious but much less potent than GAT1508 and less selective between GIRK1/2 and GIRK1/4 than GAT1508. Chlorine (GAT1501, Fig. S2D), still smaller than bromine, retained some selectivity (did not show activation of GIRK1/4 at concentrations less than 20  $\mu\text{M}$ ) but was also less potent than GAT1508 for GIRK1/2. Substituting the larger than bromine atom iodine at the 5' position (GAT 1574, Fig. S2F) proved a poorer activator than the bromine analog for both GIRK1 heteromeric channels. Finally, a methyl group substitution rather than a halogen (GAT1521, Fig. S2G) retained the specificity for brain over cardiac currents (perhaps even inhibiting the high basal cardiac currents in oocytes at higher concentrations) but with lower potency than GAT1508 for both GIRK1/2 and GIRK1/4. Substitution of bromine at positions other than the 5' of the thiophene ring (*i.e.* positions 3' GAT1570 or 4' GAT1502, Fig. S2, H and I, respectively) resulted also in much poorer activators of both GIRK1 heteromeric channels.

Wydeven *et al.* (47) demonstrated that the two critical GIRK1 residues Phe-137 and Asp-173 were necessary and sufficient for channel activation by ML297. They introduced the Phe and Asp residues in GIRK2 (GIRK2<sup>FD</sup>) and showed that the GIRK2/GIRK2<sup>FD</sup> (or GIRK2/2<sup>FD</sup>) heteromer could now be activated by ML297 (47). We utilized this GIRK2 double mutant S148F,N184D (GIRK2<sup>FD</sup>, also referred to as "GIRK1-like") in heteromers with WT GIRK2 (GIRK2/GIRK2<sup>FD</sup>) subunits as well as the corresponding GIRK4 double mutant S143F,N179D (GIRK4<sup>FD</sup>, also referred to as "GIRK1-like") in heteromers with WT GIRK4 (GIRK4/GIRK4<sup>FD</sup> or GIRK4/4<sup>FD</sup>) subunits to perform computational studies. To assess whether the binding of GAT1508 at the predicted site has any effect on the conformation of the channel gates, we monitored distances of opposite subunit residues for both the cytosolic G-loop gate (C $\alpha$  atoms

## A GIRK-specific activator in conditioned fear extinction

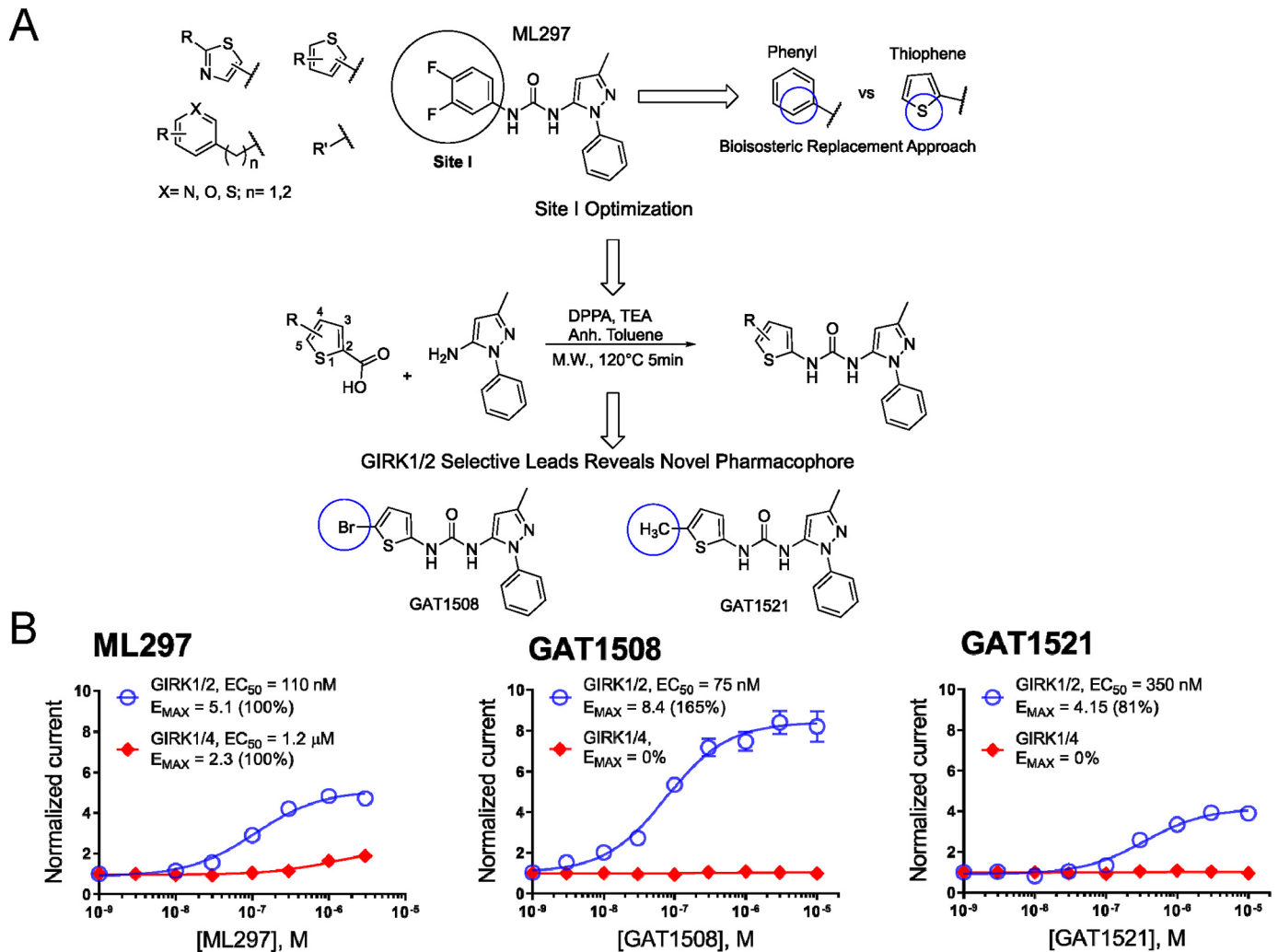


**Figure 1. ML297 derivatives that specifically activate the brain GIRK1/2 over the cardiac GIRK1/4.** *A*, shown are the rational design and the systematic focused approach to a preliminary SAR study on ML297. Assessing Site I, which is an important pharmacophore for selectivity and efficacy on GIRK1-containing channels, several analogs of ML297 were synthesized using rapid, tandem, and one-pot methodology for urea synthesis to probe their selectivity for GIRK1/2 over GIRK1/4 channels. The bioisosteric replacement strategy of the phenyl ring of Site I with a thiophene ring was adopted and found to be most tolerable and GIRK1/2 channel-selective. A thiophene ring was used as a prototype for further optimization revealing 5-bromo and 5-methyl substituents as optimal pharmacophores for GIRK1/2 selectivity, efficacy, and potency that proved better than ML297. *B*, concentration-response curves for ML297 and the selective compounds GAT1508 and GAT1521 were assessed in HEK293 cells expressing GIRK1/2 WT (blue open circle) and GIRK1/4 WT (solid red diamond) using whole-cell patch-clamp recordings. Data are mean  $\pm$  S.E. for 7–12 cells per condition. The  $EC_{50}$  of ML297 at GIRK1/2 was  $110 \pm 13$  nM, and the  $E_{MAX}$  was  $5.1 \pm 0.1$  (considered here to be 100%); at GIRK1/4 the  $EC_{50}$  was  $1.2 \pm 0.5$   $\mu$ M, and  $E_{MAX}$  was  $2.3 \pm 0.2$  (100%). At GIRK1/2 channels, GAT1508 had an  $EC_{50}$  of  $75 \pm 10$  nM, and an  $E_{MAX}$  of  $8.4 \pm 0.2$  (165% relative to the  $E_{MAX}$  of ML297), whereas GAT1521 had an  $EC_{50}$  of  $350 \pm 58$  nM, and an  $E_{MAX}$  of  $4.1 \pm 0.13$  (81% relative to the  $E_{MAX}$  of ML297).

of GIRK2–Thr-317/GIRK4–Thr-312) and the transmembrane inner helix gate (also referred to as the “helix bundle crossing-HBC gate”  $C\alpha$  atoms of GIRK2–Phe-192/GIRK4–Phe-187) during a molecular dynamics (MD) simulation (Fig. S3, A–E). In the absence of channel activators, the diameter of the G-loop gate transitioned from a pre-open state of  $\sim 15$  Å to  $\sim 10$  Å for both the GIRK2/2<sup>FD</sup> and GIRK4/4<sup>FD</sup> systems, although the HBC gate of the GIRK2/2<sup>FD</sup> system also decreased between  $\sim 10$  and  $12$  Å rapidly but to a lesser extent and more slowly in the GIRK4/4<sup>FD</sup> system. In contrast, upon ML297 binding an increase of at least  $2$  Å in the opening of the G-loop and HBC gates was observed in both systems. Consistent with our experimental results, GAT1508 could not keep the GIRK4/4<sup>FD</sup> system open as the HBC gate diameter became limiting decreasing within  $\sim 10$  ns to  $\sim 12$  Å.

### Altered binding of GAT1508 to GIRK channels underlies its specificity

We next asked the following: how is GAT1508 able to specifically activate the GIRK2-containing rather than the GIRK4-containing heteromeric channels? Analysis of the MD trajectories for the last 25 ns of the 100-ns MD simulation run showed that in the GIRK2/2<sup>FD</sup> system ML297 and GAT 1508 interacted predominantly with M1 helix residues ( $\sim 65\%$  of the interactions) compared with M2 helix residues ( $\sim 35\%$  of the interactions) (Fig. 2, A and B). Comparison of the ML297 and GAT1508 interactions with GIRK4/4<sup>FD</sup> versus GIRK2/2<sup>FD</sup> for the last 25 ns of the 100-ns MD run revealed that GAT1508 flipped its position to predominantly interact with the M2 helix (almost 65% of the interactions) compared with the M1 helix



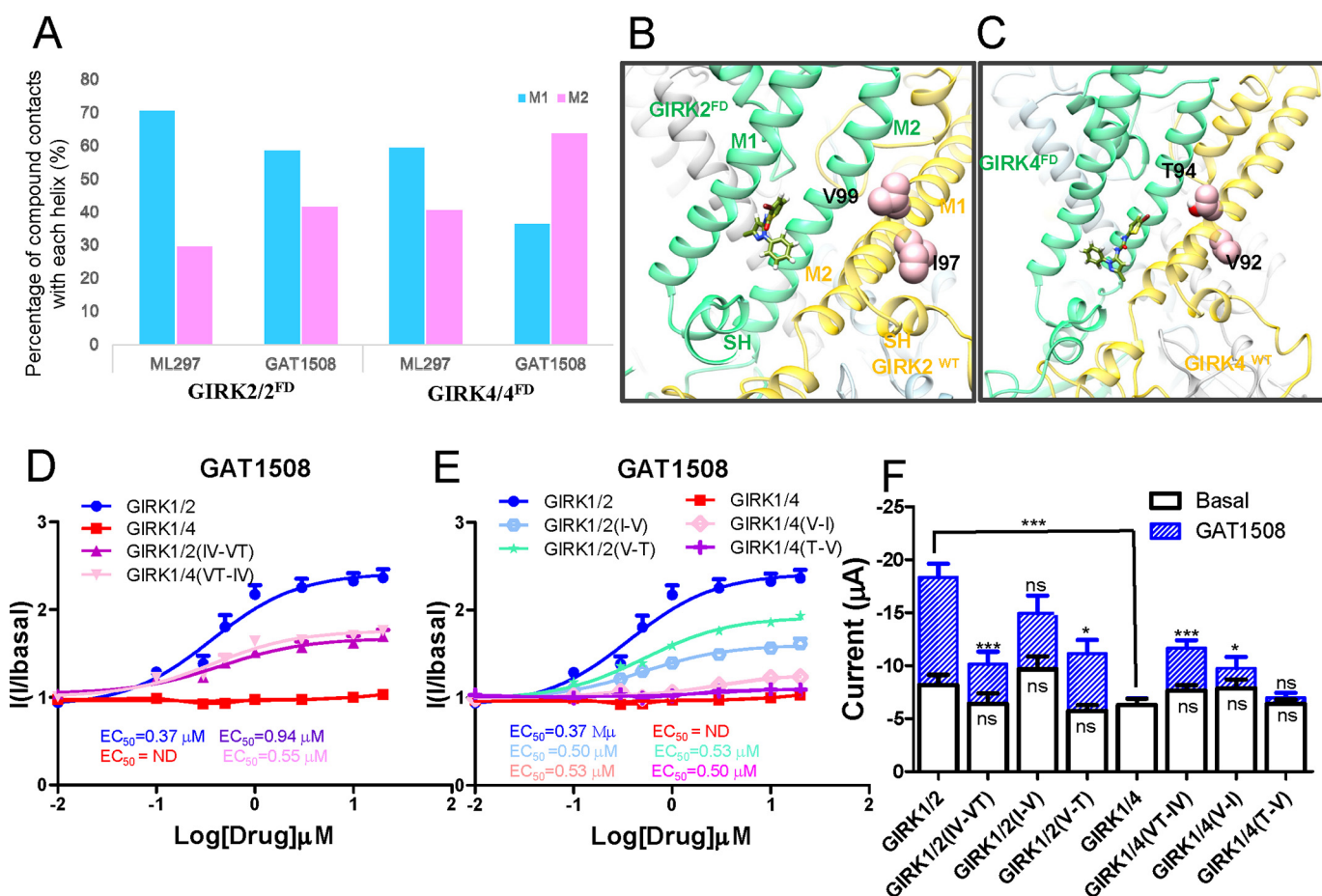


**Figure 2. Basis for selective binding of GAT1508 between brain and cardiac heteromeric channels.** A, percentage of ML297 or GAT1508 contacts with the transmembrane M1 (light blue bars) and M2 (pink bars) helices of the GIRK2/2<sup>FD</sup> and GIRK4/4<sup>FD</sup> channels during the MD trajectories. Contact was defined as drug-C $\alpha$  distance  $\leq 7$  Å. Snapshots of GAT1508 binding in GIRK2/2<sup>FD</sup> (B) and GIRK4/4<sup>FD</sup> (C) are shown. The flipping of the GAT1508 position in the GIRK4/4<sup>FD</sup> system and the proximity of the thiofuran group to the Thr-94 of the M1 helix of the WT GIRK4 subunit are shown. D, concentration-response curves of GAT1508 in GIRK1/2 (solid blue circle) and GIRK1/4 (solid red square) WT or the double mutant channels GIRK1/2(I-V-T) (purple triangle) or GIRK1/4(V-T-I) (pink inverted triangle). Data are mean  $\pm$  S.E. for 16 cells (four oocytes  $\times$  four frogs) per concentration. GAT1508 stimulated brain (GIRK1/2) heteromeric channel currents with an EC<sub>50</sub> of  $0.37 \pm 0.11$   $\mu$ M and an E<sub>MAX</sub> of  $2.42 \pm 0.07$  (considered here to be 100%). Double mutants in the GIRK2 WT subunits to corresponding GIRK4 residues showed reduced potency and efficacy for the GAT1508-induced currents with an EC<sub>50</sub> of  $0.94 \pm 0.15$   $\mu$ M and an E<sub>MAX</sub> of  $1.68 \pm 0.04$  (72% of the control GIRK1/2). Double mutants in GIRK4 WT subunits to corresponding GIRK2 residues conferred stimulation of the heteromeric channel by GAT1508 with an EC<sub>50</sub> of  $0.55 \pm 0.11$   $\mu$ M and an E<sub>MAX</sub> of  $1.76 \pm 0.03$  (75% of the control GIRK1/2). E, single mutants between brain and cardiac channels switch GAT1508 sensitivity. Concentration-response curves of GAT1508 in GIRK1/2 (solid blue circle) and GIRK1/4 (solid red square) WT or single mutant channels between unique M1 residues in GIRK2 and GIRK4: GIRK1/2(I-V) (open blue circle), GIRK1/2(V-T) (cyan star), GIRK1/4(V-I) (pink open diamond), and GIRK1/4(T-V) (blue plus). Data are mean  $\pm$  S.E. for eight cells (four oocytes  $\times$  two frogs) per concentration. GAT1508 stimulated brain (GIRK1/2) heteromeric channel currents with an EC<sub>50</sub> of  $0.37 \pm 0.11$   $\mu$ M and an E<sub>MAX</sub> of  $2.36 \pm 0.23$  (considered here to be 100%). Single mutants in the GIRK2 WT subunits to corresponding GIRK4 residues significantly reduced the potency and efficacy of the GAT1508-induced selective currents: GIRK1/2(V-T) with an EC<sub>50</sub> of  $0.53 \pm 0.07$   $\mu$ M and an E<sub>MAX</sub> of  $1.92 \pm 0.03$  (65% of the control GIRK1/2) and GIRK1/2(I-V) with an EC<sub>50</sub> of  $0.50 \pm 0.11$   $\mu$ M and an E<sub>MAX</sub> of  $1.61 \pm 0.03$  (42% of the control GIRK1/2). Single mutants in GIRK4 WT subunits to corresponding GIRK2 residues conferred stimulation of the heteromeric channel by GAT1508: GIRK1/4(V-I) with an EC<sub>50</sub> of  $0.50 \pm 0.47$   $\mu$ M and an E<sub>MAX</sub> of  $1.12 \pm 0.03$  (7% of the control GIRK1/2); GIRK1/4(V-I) with an EC<sub>50</sub> of  $0.53 \pm 0.15$   $\mu$ M and an E<sub>MAX</sub> of  $1.29 \pm 0.03$  (11% of the control GIRK1/2). F, impact of mutating GIRK2 or GIRK4 side chains predicted to lead to selective binding of the GAT1508 molecule on basal current and 20  $\mu$ M drug-induced current-enhancing effects are shown. ns signifies no significant changes in basal or drug-induced currents. Symbols denote statistical significance by one-way ANOVA. \*,  $p < 0.05$  compares WT GIRK1/2 and GIRK1/4 with GIRK1/2(V-T) and GIRK1/4(V-I), respectively. \*\*\*,  $p < 0.0005$  compares WT GIRK1/2 or GIRK1/4 with their respective double mutants,  $n = 8$ .

(almost 35% of the interactions) (Fig. 2, A and C). This was in contrast to ML297, which showed consistent binding modes with greater contacts with the M1 helix than the M2 helix for both channel heteromers. The GAT1508 flipping in the GIRK4/4<sup>FD</sup> channel positioned the thiofuran moiety pointing toward the M2 helix of the GIRK4<sup>FD</sup> subunit suggesting forming a hydrogen-halogen bond with Thr-94 (with the bromine at position 5' of the thiofuran ring) as well as hydrophobic interaction with Val-92 in the M1 helix of GIRK4 WT subunit. The volumes of the binding pockets for GAT1508 and the interacting residues are shown for GIRK2/2<sup>FD</sup> and GIRK4/4<sup>FD</sup> (Fig. S4, A–D). GIRK2 residues Ile-97 and Val-99 differ from the

corresponding GIRK4 residues Val-92 and Thr-94 in an otherwise highly conserved region between these two channel subunits (Fig. S4E). GAT1508 Site I in GIRK4/GIRK4<sup>FD</sup> comes within interaction distance of the GIRK4(T94) (Fig. S4E) and GIRK4(V92) (not shown). The distances between the Br atom of GAT1508 and the CG atom of Val-99 in the GIRK2 subunit or the OG atom of Thr-94 in the GIRK4 subunit are shown during an MD run (Fig. S4F). In the first 5 ns of this run, a distance around 5 Å suggests a direct halogen-hydrogen bond between GAT1508 and Thr-94. In the last 50 ns of the MD run, the mean distance between the Br atom of GAT1508 and the OG atom of Thr-94 around 6.39 Å suggests that a hydrogen-

## A GIRK-specific activator in conditioned fear extinction

halogen bond may be stabilized by some other nearby donor residue (73, 74). In the GIRK2/2<sup>FD</sup> case, this distance stabilized around 12 Å throughout the MD run. However, because of limitations using a molecular mechanics force field, more accurate estimates of hydrogen–halogen proximity will require future quantum mechanical studies. Double (Fig. 2D) and single (Fig. 2E) mutations demonstrated that these residue differences accounted in part for the selectivity of GAT1508 for GIRK1/2 over GIRK1/4, decreasing or increasing the efficacy and potency of the two WT heteromers, respectively. The raw summary currents for single and double mutants are shown and compared for statistical significance to the WT basal and GAT1508-induced currents (Fig. 2F).

### GAT1508-binding site

We next proceeded to validate the modeling results of the GAT1508-binding site and the role of the critical Phe and Asp residues. We first studied computationally in GIRK2/2<sup>FD</sup> the GAT1508 detailed interactions of Sites I, II, and IV with M1 and M2 residues. We then proceeded to validate experimentally the computational predictions through mutagenesis in GIRK1/2 heteromers. The two critical Phe and Asp residues (Phe-137 and Asp-173 in GIRK1) are distant from each other, with the GIRK2 Phe-148 in the inaccessible pore helix and unlikely to directly interact with ML297. Thus, our docking box for GAT compounds was first set around Asp-184 in the GIRK2<sup>FD</sup> subunit, a good template requiring only a minor change from the experimentally-determined structure (20) for docking studies and MD simulations.

In this model, Site I engaged in a  $\pi$  network formed among three Phe residues: Phe-108, Phe-109, and the critical Phe-148 in the GIRK2<sup>FD</sup> subunit (Fig. 3A, middle panel). We monitored the frequency distributions of the distances and interface angles between the aromatic rings of the Phe residues and the thiophene ring of the GAT1508 Site I. Distances less than 6–7 Å are consistent with  $\pi$ -stacking interactions, and interphase angles of 60–90° between two aromatic rings are considered to form T-stacking interactions that are weaker than  $\pi$ -stacking interactions (48–50), whereas an interphase angle less than 30° indicates parallel  $\pi$ -stacking (Fig. 3A, right panel). The thiophene ring of Site I showed stronger interactions with Phe-108 than Phe-109 (Fig. 3, B and E), whereas the angles between the thiophene ring of Site I and Phe-108 or Phe-109 showed mostly distributions around 60–90°, indicating T-stacking interactions (Fig. 3, C and F). The binding of GAT1508 stabilized interactions between Phe-108 and Phe-109 (shifted distributions to shorter distances and larger angles forming T-stacking interactions) (Fig. 3, D and G), while it maintained the  $\pi$ -stacking interaction distances and shifted the distribution of interface angles between Phe-109 and Phe-148 to be centered around 30° forming parallel  $\pi$  interactions (Fig. 3, H and I). Mutation of the conserved Phe GIRK1 residue corresponding to the GIRK2–Phe-108 (corresponding residue number in GIRK1 is 11 amino acids less than the GIRK2 residue number), GIRK1(F97A) resulted in a significant decrease in the GAT1508-induced current over the mutant basal current. Thus, these results provide evidence that the GAT1508 Site I stabilizes the network of interactions of the

M1 residue GIRK2<sup>FD</sup>(Phe-108) (or GIRK1(Phe-97)) with GIRK2<sup>FD</sup>(Phe-148) (or GIRK1(Phe-137)).

The GAT1508 Site II was predicted to interact with M1 GIRK2<sup>FD</sup> subunit residues Val-104 and Val-101 and M2 GIRK2<sup>FD</sup> subunit residue Leu-179 (Fig. 4A). Mutagenesis of the corresponding M1 GIRK1 residues Thr-90 and Val-93 and the M2 GIRK1 residue Leu-168 to either a similar residue or to Gly yielded significant changes in GAT1508-induced currents over basal currents (Fig. 4, B and C). In the case of GIRK1(Val-93) changing the hydrophobic residue to a polar one (V93S) yielded a significant decrease in GAT1508-induced activity over basal. Removal of the GIRK1(Thr-90) or (Leu-168) side chains T90G or L168G produced significant increases in the GAT1508-stimulated current over basal, although the conserved mutations (T90S or L168V) had no significant effect. Thus, these results support the predicted residue interactions with the GAT1508 Site II.

The GAT1508 Site IV revealed that a conserved Tyr residue (GIRK2(Tyr-102) and GIRK1(Tyr-91)) toggles between the two critical GIRK1 residues of interaction, Phe-137 and Asp-173.

The benzene ring of Site IV of GAT1508 engaged in T-stacking interactions with the M2 residue Phe-186 of the GIRK2<sup>FD</sup> subunit (Fig. 5, B and C). As a result, the conserved M1 residue GIRK2<sup>FD</sup>(Tyr-102) moved closer to the M2 residue Asp-184 of the GIRK2<sup>FD</sup> subunit to form a hydrogen bond (Fig. 5F) and farther away from Phe-148 (from a distance of 6 Å to one of 10 Å, which destabilized the  $\pi$  interaction, and we assumed an interface angle distribution centered around 60°) (Fig. 5, D and E). Mutagenesis of GIRK1(D173N) abolished GAT1508-induced GIRK1/2 currents, whereas mutation of the GIRK1 residue corresponding to GIRK2<sup>FD</sup>(Phe-186) to an Ile residue (*i.e.* GIRK1(F175I)), which is highly conserved in Kir channels other than GIRKs, also caused a significant reduction in GAT1508-induced currents over basal (Fig. 5, G and H). Thus, these results support the notion that the GAT1508 Site IV benzene forms  $\pi$ -stacking interactions with GIRK2<sup>FD</sup>(Phe-186) (or GIRK1(Phe-175)), which allows GIRK2(Tyr-102) (or GIRK1(Tyr-91)) to hydrogen-bond with the GIRK2<sup>FD</sup>(Asp-184) (or GIRK1(Asp-173)) moving it away from the  $\pi$  interactions it shared with the GIRK2<sup>FD</sup>(Phe-148) (or GIRK1(Phe-137)).

Altogether, our experimental validation gives us confidence in this model of the GAT1508-binding site. From the  $\pi$  network of interactions of the bromothiophene on Site I through the hydrophobic urea interactions of Site II to the  $\pi$  interactions of the benzene ring of Site IV with a highly-conserved M2 helix Phe residue, the simulations predict a critical role for an M1 Tyr residue conserved in GIRK channels (Tyr-91 in GIRK1) that connects the critically-required two residues of GIRK1 (Phe-137 and Asp-173) to switch in the presence of GAT1508 to hydrogen bond more strongly with the critical M2 Asp residue. These results provide an insight of how these distant two critical residues are required for activation by the urea-based compounds.

### Activation effects of selective GAT compounds relate to channel-PIP<sub>2</sub> interactions

GAT1508 binds 10–16 Å away from the PIP<sub>2</sub> head group interacting with the adjacent subunit (see Fig. 6B). To gain structural insights whether the binding of GAT1508 and

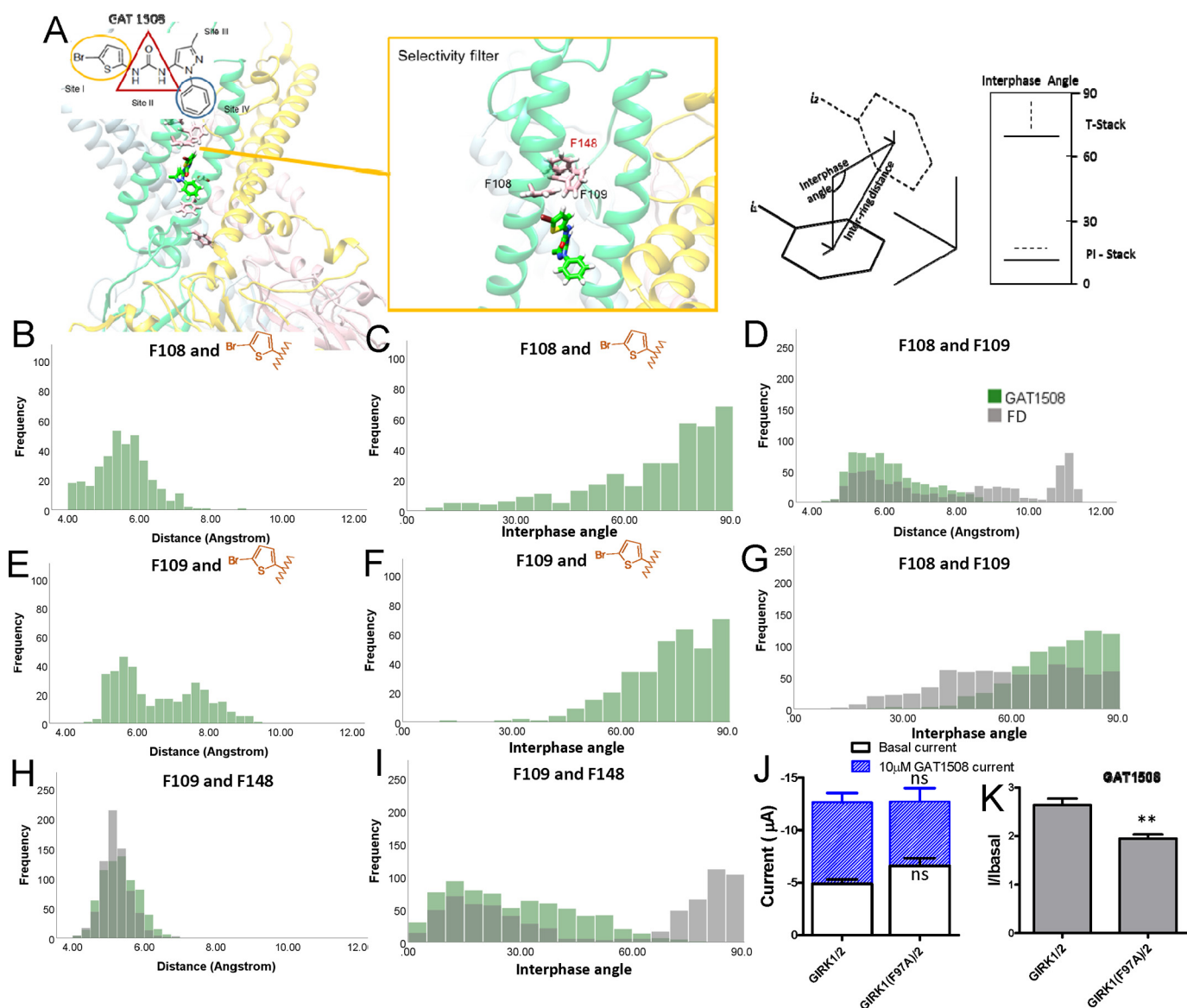


**Figure 3.** Site I of GAT1508 binding joins into the  $P_i$  network system around pore helix of GIRK1-like subunit and single mutant functional effects. *A, right*, binding site of GAT1508 in the GIRK2<sup>FD</sup> subunit (GAT subunit is shown in green; adjacent WT subunit is shown in yellow, and nondrug-binding subunits are shown in gray). *Left*, zooming in on Site I of the GAT1508-binding site (yellow outlines) reveals  $P_i$  interactions of the compound with residues Phe-108 and Phe-109 in the M1 helix of the GIRK2<sup>FD</sup> subunit. The  $P_i$  network was monitored during the MD simulation and displayed by plotting the distance and interphase angle frequency distributions between GAT1508 and Phe-108 (B and C) between GAT1508 and Phe-109 (E and F) between Phe-108 and Phe-109 (D and G), and between Phe-109 and Phe-148 (H and I) in GIRK2/2<sup>FD</sup> in the absence of the compound (black) or with GAT1508 (olive green). The plane interphase angle was calculated as the cross-product of the normal vectors of each aromatic ring. The impact of mutations of GIRK1 side chains predicted to bind the GAT1508 molecule on basal currents and on the 10  $\mu$ M drug-induced current-enhancing effect (J) and normalized drug-induced effect (K). Symbols denote statistical significance by one-way ANOVA. \*\*,  $p < 0.005$  compares WT GIRK1/2 with GIRK1(F97I)/2.  $n = 8$ .

ML297 compounds (Fig. 2) opened the channel gates (Fig. S3) by strengthening channel-PIP<sub>2</sub> interactions, we conducted MD simulations to further investigate possible differences between brain and cardiac channels in the PIP<sub>2</sub>-binding area. The movement of compounds and PIP<sub>2</sub> relative to the channel was monitored to explore the binding stability in each heteromeric system during the simulation. Compared with the channels without ligand, binding of PIP<sub>2</sub> did not introduce major structural changes. In contrast, binding of the activating compounds showed significant changes in channel-PIP<sub>2</sub> interactions. To quantify these interactions, the normalized salt-bridge formation between the head group of PIP<sub>2</sub> and the positively-charged channel residues was generated during the

MD simulation without any ligand (Fig. 6, A and B) or in the presence of ML297 or GAT1508 for each of the GIRK2/2<sup>FD</sup> and GIRK4/4<sup>FD</sup> systems (Fig. 6A). The interaction between channel and PIP<sub>2</sub> increased by ~61–73% in the presence of each compound in the GIRK2/2<sup>FD</sup> heteromeric channel. In the case of the GIRK4/4<sup>FD</sup> heteromeric channel simulation, however, ML297 increased channel-PIP<sub>2</sub> interactions by ~38%, whereas GAT1508 showed a much lower (~18%) increase in channel-PIP<sub>2</sub> interactions. To test experimentally these model predictions, we pursued experiments in inside-out macropatches that enable dose-response experiments with the synthetic soluble PIP<sub>2</sub> analog diC8-PIP<sub>2</sub>. Fig. 6C shows results from inside-out macropatches of GIRK1/2 expressed in *Xenopus* oocytes, where



## A GIRK-specific activator in conditioned fear extinction

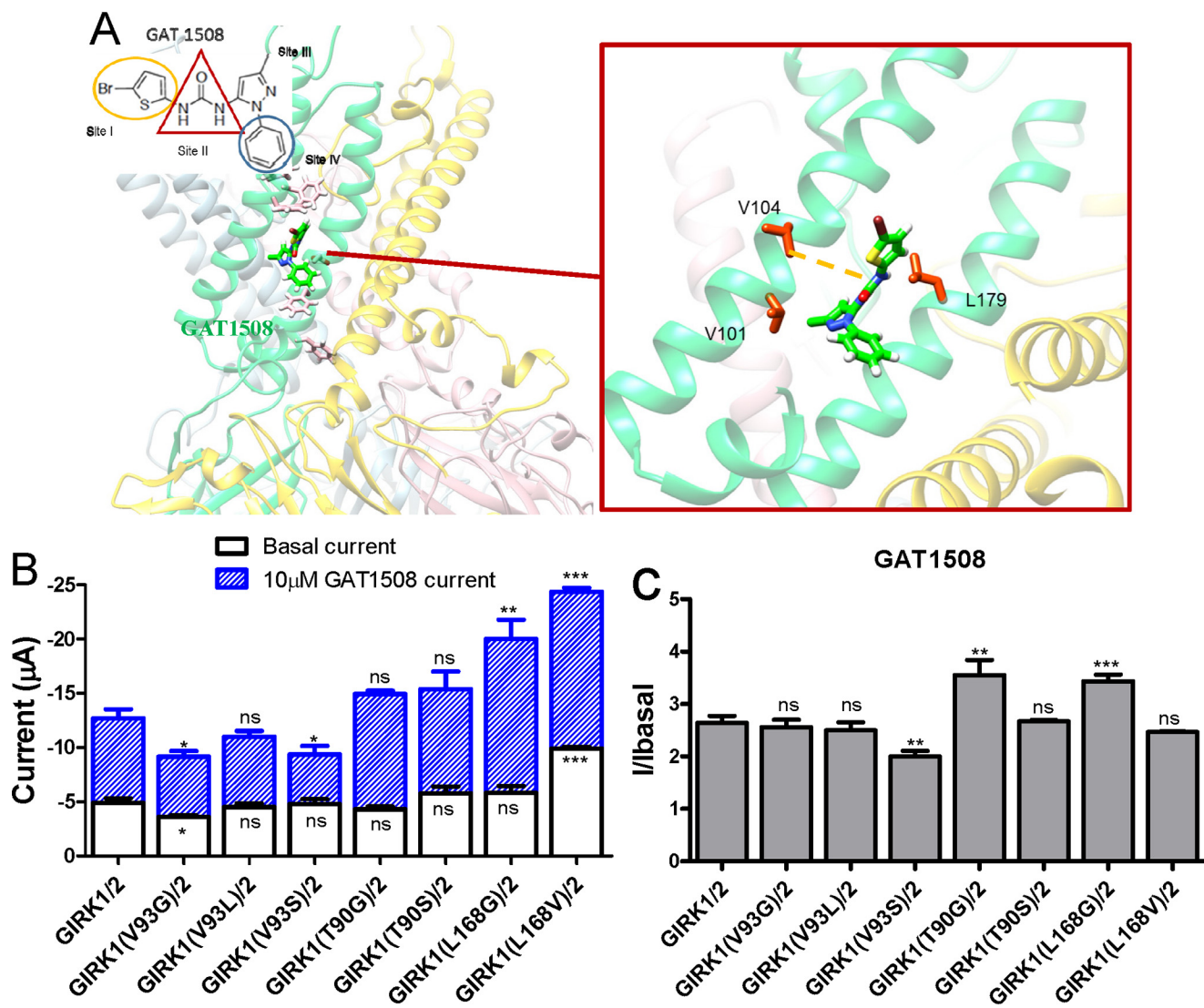


**Figure 4. Predictions of GAT1508 Site II interactions with residues in the middle of the M1 helix in the GIRK1-like subunit probed by point mutations.** *A, right*, binding site of GAT1508 in the GIRK2<sup>FD</sup> subunit (FD subunit is shown in green; adjacent WT subunit is shown in yellow, and nondrug-binding subunits are shown in gray). *Left*, zooming in on the GAT1508-binding Site II (red outlines) shows hydrophobic interactions of the compound with residues Val-104 and Val-101 (on the M1 helix) and Leu-179 (on the M2 helix). *B*, impacts of these GIRK2<sup>FD</sup> side chains on basal current and 10 µM drug-induced current were probed with corresponding mutations on GIRK1 (numbers of residues 11 less than GIRK2: Val-93, Thr-90, and Leu-168) that either preserved the hydrophobic or hydrophilic property of the residue or removed the side chain with a Gly residue (*C*), normalized drug-induced current over basal current. Results from GIRK1(Val-93L)/2, GIRK1(Val-93S)/2, GIRK1(Val-93G), GIRK1(T90G)/2, GIRK1(T90S)/2, GIRK1(L168G)/2, and GIRK1(L168V) are shown. Symbols denote statistical significance by one-way ANOVA. \*,  $p < 0.05$  compares WT GIRK1/2 and GIRK1(Val-93G)/2 for basal current and drug-induced current, and GIRK1(Val-93S)/2 for drug-induced current, respectively. \*\*,  $p < 0.005$  compares WT GIRK1/2 with GIRK1(V93S)/2 and GIRK1(T90G)/2 for normalized drug-induced current, and GIRK1(L168G)/2 for drug-induced current. \*\*\*,  $p < 0.0005$  compares WT GIRK1/2 with GIRK1(L168V)/2 for basal current and drug-induced current, and with GIRK1(L168G)/2 for normalized drug-induced current.  $n = 8$ .

diC8-PIP<sub>2</sub> dose-dependent activity (NPo) from control patches in the absence of any compound was compared with those from patches exposed to 10 µM of ligand (ML297 or GAT1508). GAT1508 was more potent and efficacious in sensitizing the channel to PIP<sub>2</sub> activation than ML297. Fig. 6D shows results from the analogous experiments with GIRK1/4. Only ML297 was able to left-shift the sensitivity of GIRK1/4 heteromers to PIP<sub>2</sub>, whereas GAT1508 was ineffective in changing the sensitivity of these heteromers to PIP<sub>2</sub>. We also pursued whole-cell patch-clamp experiments to further validate the model predictions from the excised-patch results. Expression of a light-activated phosphatase, which upon exposure to blue light dephosphorylates PIP<sub>2</sub> to phosphatidylinositol 4-phosphate (51) and

inhibits GIRK currents, allowed recording of macroscopic currents in the absence and presence of ML297 and the brain-specific GAT1508. Indeed, time courses of current inhibition upon stimulation of light-activated phosphatase showed increasing protection from current inhibition with GAT1508 > ML297 > control for GIRK1/2-expressing HEK293 cells both for current levels and kinetics of inhibition (Fig. 7). These results were in marked contrast to GIRK1/4 currents, where only ML297 but not GAT1508 was able to provide protection of currents from inhibition by the light-activated phosphatase (Fig. 7, E and F).

Because GAT1508 and ML297 only bind GIRK1 or GIRK1-like (*i.e.* “FD-containing”) subunits resulting in corresponding

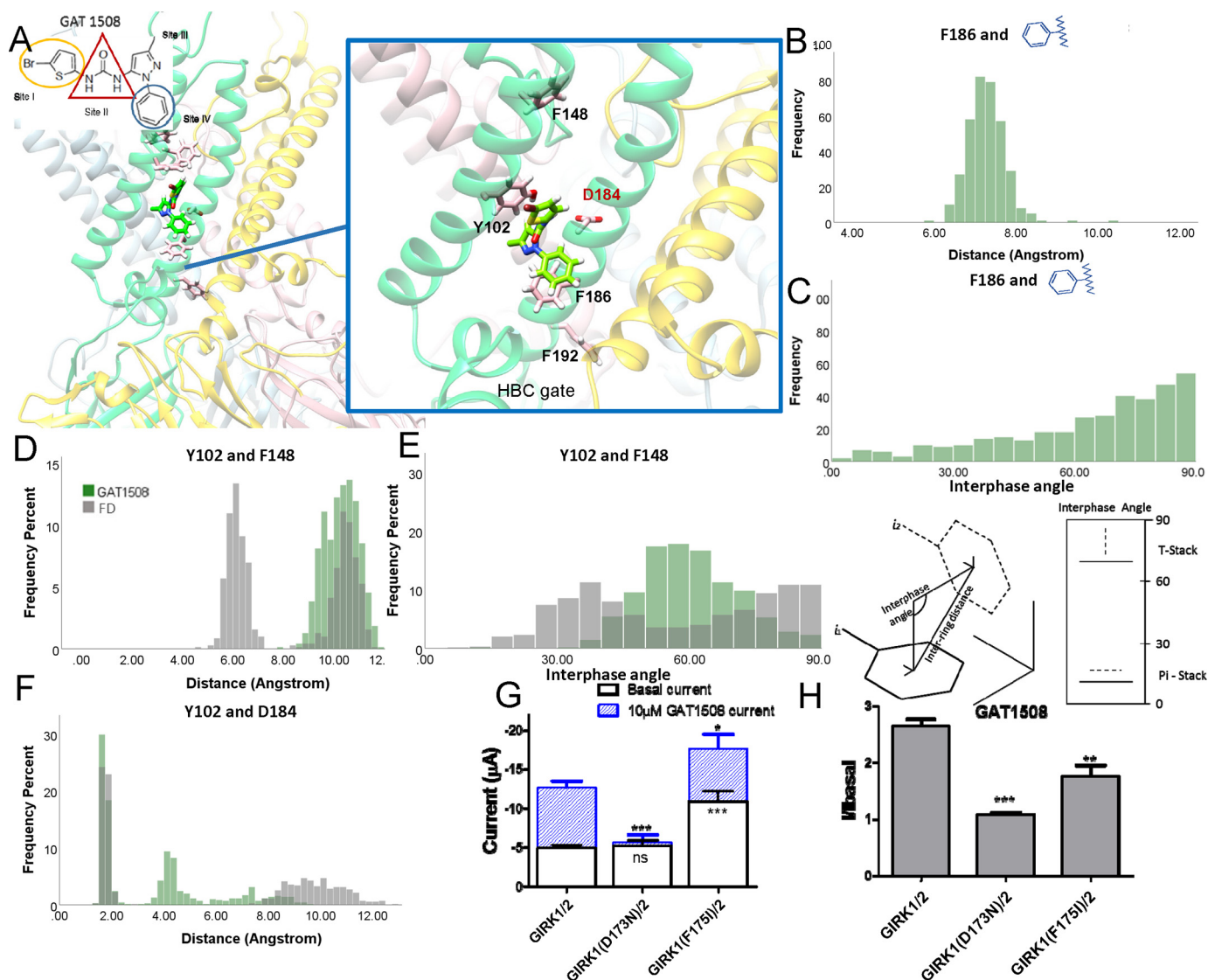


**Figure 5. Probing predicted GAT1508 Site IV interactions with the intracellular side of M2 helix in the GIRK2<sup>FD</sup> subunit with point mutants.** *A, right*, binding site of GAT1508 in the GIRK2<sup>FD</sup> subunit (FD subunit is shown in *green*; adjacent WT subunit is shown in *yellow*, and nondrug-binding subunits are shown in *gray*). *Left*, zooming in on the GAT150-binding Site IV (*blue outlines*) reveals  $P_i$  interactions of the compound with GIRK2<sup>FD</sup> residue Phe-186. The interaction network was monitored during the MD simulation (distance and interface angle) as frequency distributions between GAT1508 Site IV and Phe-186 (*B and C*), between Tyr-102 and Phe-148 (*D and E*), and between Tyr-102 and Asp-184 in GIRK2/2<sup>FD</sup> in the absence of the compound (*black*) or with GAT1508 (*olive green*). The plane interphase angle is calculated as the cross-product of the normal vectors of each aromatic ring. When this interphase angle is between 60 and 90, the two aromatic rings form a T stack. When the interphase angle is less than 30, they form traditional  $\pi$ -stacking interactions. *B and C*, angles between the GAT1508 benzene ring of Site IV and Phe-186 show a broad distribution with a peak at 90, suggesting T-stacking interactions. *D–F*, GAT1508 binding destabilizes the Phe-148 interaction with Tyr-102, releasing it to form H-bond interactions with Asp-184. *G and H*, impact of probing these predictions with corresponding mutations on GIRK1 (e.g. F175I and D173N) is significant. Symbols denote statistical significance by one-way ANOVA. \*,  $p < 0.05$  compares WT GIRK1/2 and GIRK1(F175I)/2 in drug-induced current. \*\*,  $p < 0.005$  compares WT GIRK1/2 and GIRK1(F175I)/2 in normalized drug-induced current. \*\*\*,  $p < 0.0005$  compares WT GIRK1/2 with GIRK1(D173N)/2 drug-induced current and normalized drug-induced current and with GIRK1(F175I)/2 basal current.  $n = 8$ .

changes in channel-PIP<sub>2</sub> interactions and channel activity, we next sought to compare channel subunit-specific interactions with PIP<sub>2</sub> for subunits bound to the ligand (P-FD) *versus* those not bound to the ligand (P-WT) (Fig. 8, *A and B*). We calculated the normalized salt-bridge formation between P-FD and P-WT subunits in the GIRK2/2<sup>FD</sup> and GIRK4/4<sup>FD</sup> systems and found that the binding of ML297 or GAT1508 in the “FD-containing” subunits shifted the neighboring subunit PIP<sub>2</sub> binding and increased P-WT interactions with the GIRK2 or GIRK4 WT subunits (see Fig. 8*B*). In fact, the probability of salt bridges between channel and PIP<sub>2</sub> increased more in the GIRK2 than in GIRK4 subunits. In contrast, the compounds decreased the

channel P-FD interactions in the FD-containing subunits for both heteromeric channels and perhaps somewhat more for GIRK4/4<sup>FD</sup> than GIRK2/2<sup>FD</sup> heteromers. Thus, the overall changes ( $P_{WT} - P_{FD}$ ) in channel-PIP<sub>2</sub> interactions by GAT1508 showed increases only in GIRK2/2<sup>FD</sup> heteromers, consistent with the changes in overall interactions discussed in Fig. 6*A*.

#### Ligand-induced changes in specific channel-PIP<sub>2</sub> interactions

To identify changes in specific channel residue interactions with PIP<sub>2</sub> upon ligand binding, we carried out principal component analysis (PCA) in the presence and absence of ML297 and GAT1508. The PCA analysis implicated changes in the



## A GIRK-specific activator in conditioned fear extinction

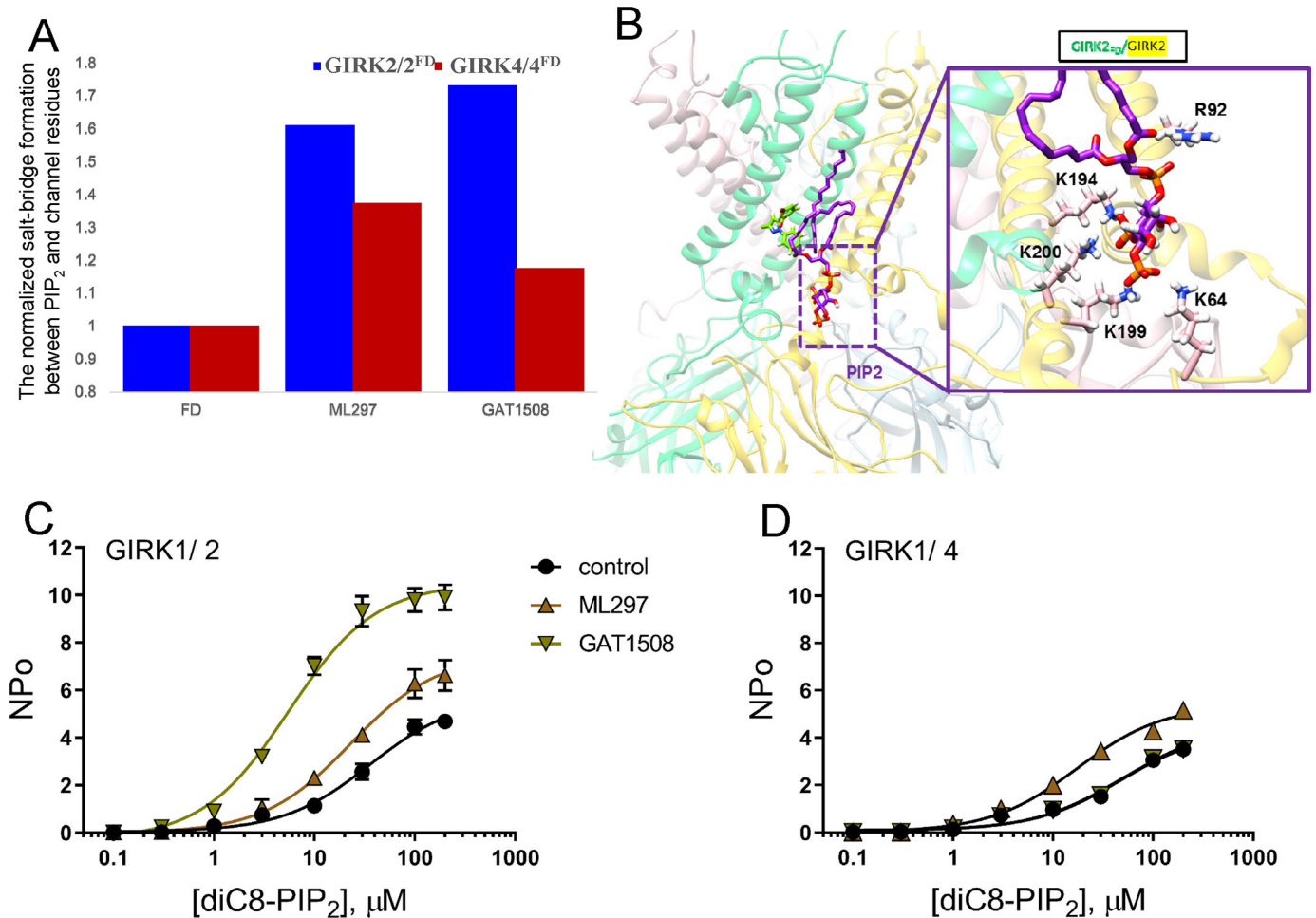


**Figure 6. Specific activation by GAT compounds increases brain GIRK2 but not cardiac GIRK4 channel-PIP<sub>2</sub> interactions.** A and B, normalized salt-bridge formation between the head group PIP<sub>2</sub> and positively-charged channel residues are calculated during the last 25 ns of the 100-ns MD simulation runs in the absence of ligand or with ML297 and GAT1508 bound in the GIRK2/2<sup>FD</sup> (blue) and GIRK4/4<sup>FD</sup> (red) systems. C, GIRK1/2 channel NPo was assessed by diC8-PIP<sub>2</sub> concentration-response curves using inside-out macropatches from *Xenopus* oocytes in the presence and absence of 10 μM ML297 or GAT1508; data are means ± S.E. for 5–6 patches per condition. When studied under control conditions (black solid circle), GIRK1/2 channels showed an apparent affinity to diC8-PIP<sub>2</sub> of 36 ± 7 μM and an E<sub>MAX</sub> of 5.7 ± 0.3 (100%). ML297 (brown solid triangle) increases the apparent affinity to 23 ± 5 μM and the E<sub>MAX</sub> to 7.5 ± 0.4 (100%). GAT1508 (olive green inverted solid triangle) increased the apparent affinity and E<sub>MAX</sub> further to 5.5 ± 7 and 10.5 ± 0.3 μM (184%), respectively. D, under control conditions, GIRK1/4 channels had an apparent affinity for diC8-PIP<sub>2</sub> of 48.4 ± 8 μM and an E<sub>MAX</sub> of 4.4 ± 0.2 (100%). ML297 increased the apparent affinity to 17.4 ± 2 μM and raised the E<sub>MAX</sub> to 5.4 ± 0.2 (123% of the control). In contrast, treatment with GAT1508 did not change the apparent affinity for diC8-PIP<sub>2</sub> from control (46 ± 7.4 μM) or the efficacy (98.6 and 103%, respectively).

Slide (or interfacial) helix interactions with PIP<sub>2</sub> upon ligand (ML297 or GAT1508) binding in GIRK2/2<sup>FD</sup> or ML297 in GIRK4/4<sup>FD</sup> (Fig. S5). Interestingly, although GAT1508 induced changes in the M1 helix of the GIRK4<sup>FD</sup> subunit, these changes were not transduced to the M2 and Slide helices (Fig. S5D). Polar interactions could be formed between GIRK2<sup>FD</sup>(Tyr-76) and GIRK4<sup>FD</sup>(Tyr-71) with the P(4,5) of PIP<sub>2</sub> when ML297 was bound to the same subunit as the Tyr residue (Fig. 8, C, top, and D). In contrast, when GAT1508 was bound, this interaction was retained by GIRK2<sup>FD</sup> but not GIRK4<sup>FD</sup> (Fig. 8, C, bottom, and D). The corresponding GIRK1(Ser-65) residue (Fig. 8E) could be serving the same role in stabilizing the phosphoinositol head group for interactions with nonligand-binding subunits.

To test the prediction of the model that GIRK1(Ser-65) could be a residue in the ligand-binding subunit that critically affects channel-PIP<sub>2</sub> interactions, we produced two mutants at this position, an Ala mutation that would be predicted to abolish the ability to strengthen channel-PIP<sub>2</sub> interactions or a Tyr residue

(like in the GIRK2<sup>FD</sup> and GIRK4<sup>FD</sup> simulations) that should enable channel-PIP<sub>2</sub> interactions. We tested each of these mutants and compared them with the WT GIRK1 as part of heteromeric channels with GIRK4 in the presence and absence of GAT1508 or ML297, using the light-activated phosphatase assay introduced in Fig. 7. The GIRK1(S65A) decreased, whereas the GIRK1(S65Y) increased channel-PIP<sub>2</sub> interactions in the GIRK1/4 heteromer (Fig. 9A). Interestingly, the activators showed no effect in either the current remaining or the kinetics of inhibition by the light-activated phosphatase in the GIRK1(S65A)/4 mutant heteromers failing to strengthen channel-PIP<sub>2</sub> interactions, whereas no significant effect by the activators could be obtained in the already enhanced channel-PIP<sub>2</sub> interactions of the GIRK1(S65Y)/4 mutant heteromers (Fig. 9, B and C). These results support the model predictions for the importance of GIRK1(Ser-65) in its ability to form polar interactions with the PIP<sub>2</sub> phosphates and position the PIP<sub>2</sub> head group for interactions with the GIRK2 or GIRK4 subunits.

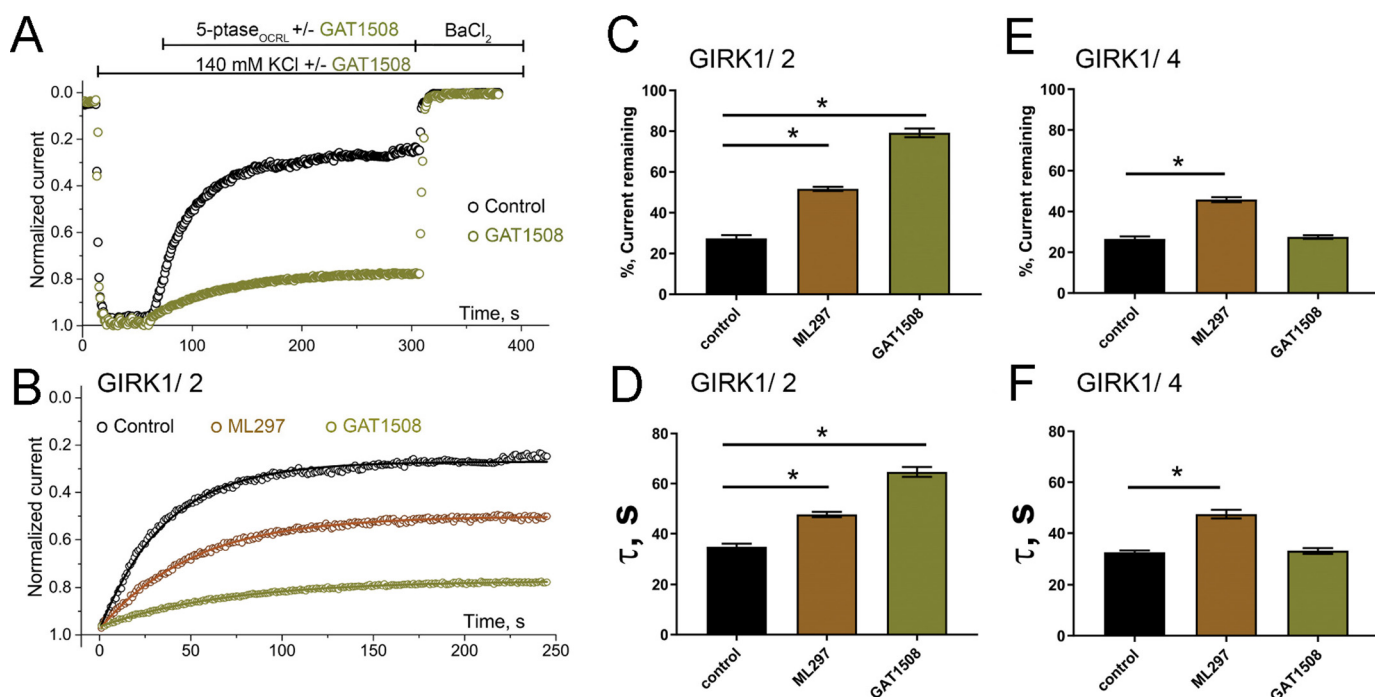


**Figure 7. ML297 and GAT1508 protect the increasing channel activity from inhibition by PIP<sub>2</sub>-dephosphorylating light-sensitive phosphatase.** Data are currents recorded from HEK293 cells using patch-clamp in the whole-cell mode and are shown as means  $\pm$  S.E. for 6–8 cells per group. Statistical significance was calculated using unpaired *t* tests. \*, *p* < 0.01. *A*, representative plots of normalized current magnitude against time show that GIRK1/2 channel current decreases in response to light-activated dephosphorylation of PIP<sub>2</sub> by the phosphatase 5-ptase<sub>OCRL</sub> (control, black open circle). The decrease in current is reduced when GIRK1/2 channels are studied in the presence of 10  $\mu$ M GAT1508 (olive green open circle). *B*, 5-ptase<sub>OCRL</sub>-mediated decrease in GIRK1/2 current is characterized by mono-exponential fits in the presence and absence of 10  $\mu$ M ML297 (brown open circle) or GAT1508 (olive green open circle). ML297 and GAT1508 increase to a different degree the percentage of GIRK1/2 channel current remaining following activation of 5-ptase<sub>OCRL</sub> (*C*) and increase the  $\tau$  of current inhibition to a different extent (*D*). ML297, but not GAT1508, increases the percentage of residual GIRK1/4 channel current (*E*) and the  $\tau$  of the current decrease, following activation of 5-ptase<sub>OCRL</sub> (*F*).

Root mean square fluctuation–C $\alpha$  root mean square fluctuation analysis was also carried out as a measure of flexibility induced by each of ML297 and GAT1508 during MD simulations. Compared with ligand-free or the bound ML297, binding of GAT1508 increased the flexibility of the N terminus of the GIRK4<sup>FD</sup>-containing subunits (Fig. S6B) more than the corresponding GIRK2 subunits (Fig. S6A). The crystal structure of GIRK2 in complex with PIP<sub>2</sub> has revealed that Lys-64 is part of the PIP<sub>2</sub>-binding site for this channel (see Fig. 6B) (20). During the MD simulation of both GIRK2 and GIRK4 heteromeric channels in the absence of ligands (labeled FD), the side chain of Lys-64/Lys-59 in the N terminus of GIRK2/GIRK4 adopted an upward orientation and formed interactions with the phosphate group of PIP<sub>2</sub>, similar to those seen in the GIRK2-PIP<sub>2</sub> co-crystal structure (Fig. S6, C and G). In the presence of ML297, the N terminus of GIRK2 and the GIRK4<sup>FD</sup>-containing subunit appeared to be more stable. Thus, in addition to the Lys-64/Lys-59, the Arg-60/Lys-56 residue also moved upward forming a new salt bridge with PIP<sub>2</sub> in both heteromeric channels (Fig. S6, D and H). GAT1508 binding in GIRK2 heteromeric channels also increased channel-PIP<sub>2</sub> interactions, and PIP<sub>2</sub> now interacted with Lys-64 and Arg-60 simultaneously in both the FD and WT subunits (Fig. S6, E and F). In contrast, in the GIRK4 heteromeric channel, the binding site of GAT1508 was shifted, partially losing its ability to regulate the M1 helix. Coincident with this change, the N terminus showed an increase in its flexibility moving downward, forcing PIP<sub>2</sub> to lose its interaction with both Lys-56 and Lys-59 in the FD-contain-

ing subunits (Fig. S6I) but not with the corresponding residues in the WT subunits (Fig. S6J). These predictions of the model could also be contributing to the decreased channel-PIP<sub>2</sub> interactions (see Figs. 6 and 7) caused by GAT1508 in GIRK1/4 relative to GIRK1/2 channels.

#### GIRK1/2-selective GAT1508, unlike ML297, shows no cardiac or cardiovascular effects *ex vivo* or *in vivo*

GIRK channels are widely expressed in the brain and in the heart; however, the distribution of the GIRK1/4 is predominantly in the heart, whereas GIRK1/2 channels are more restricted to the central nervous system (1, 31). As our SAR and *in vitro* studies suggest that GAT1508 is more selective for GIRK1/2 channels, we investigated the cardiovascular effects of GAT1508 *versus* the less selective ML297 in freely-moving animals implanted with radio telemetry probes. Rats injected with ML297 (30 mg/kg) demonstrated paradoxical long-lasting increases in heart rate (HR, treatment effect  $F_{2,16} = 5.6$ , *p* = 0.014, time effect  $F_{51,816} = 2.66$ , *p* < 0.0001, repeated measures (RM) ANOVA (Fig. S7A) and mean arterial pressure ( $\Delta$ MAP, treatment  $\times$  time interaction  $F_{102,816} = 1.4$ , *p* = 0.01, RM ANOVA, Fig. S7B) without significantly affecting locomotor activity ( $\Delta$ LA, treatment effect *p* = 0.7, Fig. S7C) or body temperature ( $\Delta$ BT, treatment effect *p* = 0.2, Fig. S7D). In contrast, animals treated with GAT1508 (30 mg/kg) showed no significant changes in cardiovascular parameters or motor activity (Fig. S7, A–D). The persistent paradoxical increases in the *in vivo* heart rate by ML297 prompted us to compare the effects of

## A GIRK-specific activator in conditioned fear extinction

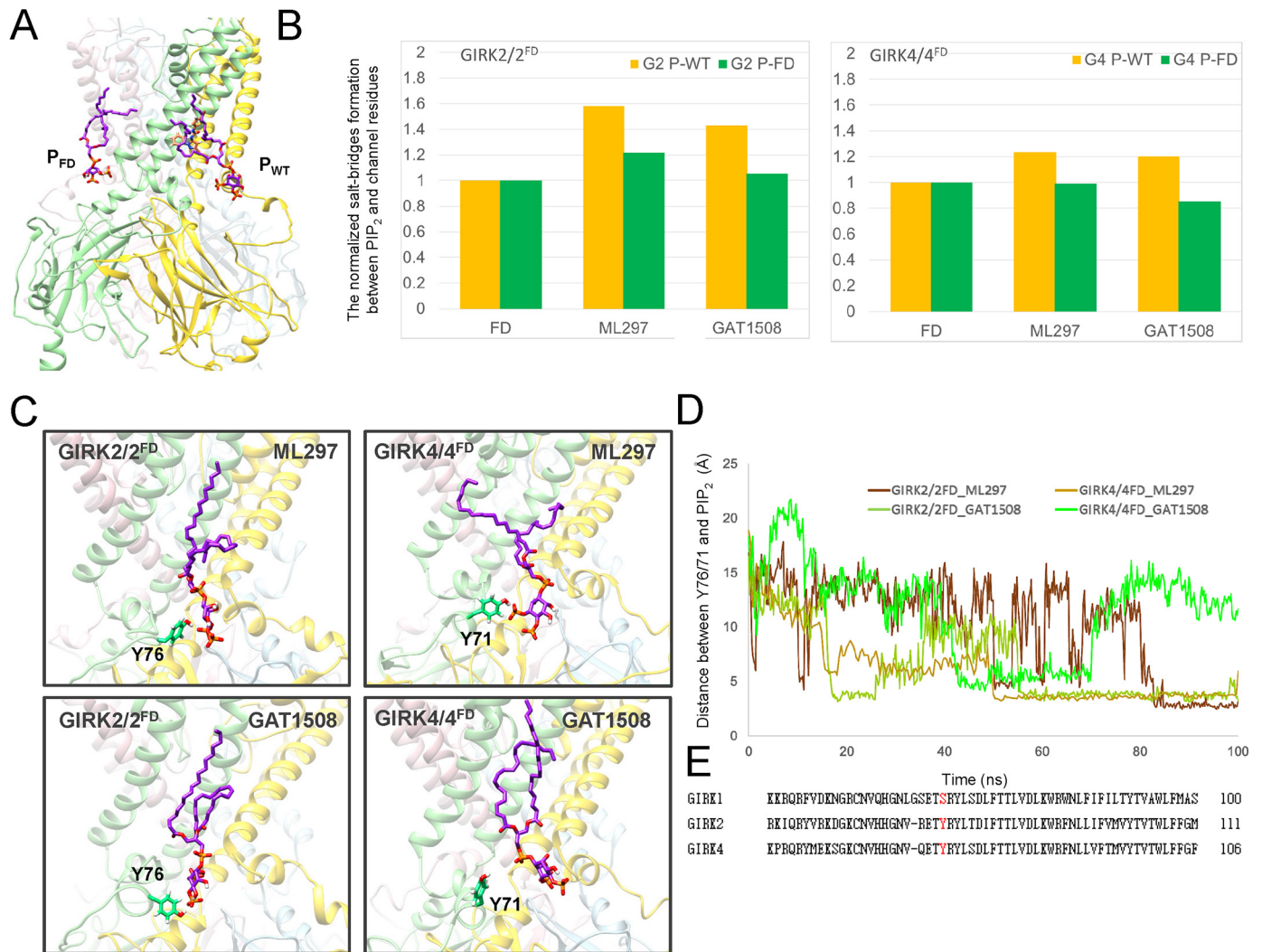


**Figure 8. GAT1508 binding to the FD-containing subunits induces a smaller increase in the adjacent (non-FD or WT) subunit in GIRK4 than in GIRK2 via a critical Slide helix-specific polar interaction.** *A*, based on the PIP<sub>2</sub>-binding area, we classified PIP<sub>2</sub> into two types. *P-WT* (yellow) represents the two PIP<sub>2</sub> molecules interacting with WT (nondrug binding on non-FD containing) subunits around the area that drugs bind when present. *P-FD* (green) represents the two PIP<sub>2</sub>-interacting molecules with the FD-mutated drug-binding subunits (analogous to GIRK1) in the absence of drugs bound. *B*, percentage of salt-bridge formation between each type of PIP<sub>2</sub> (*P-WT* and *P-FD*) and positively-charged channel residues in GIRK2/2<sup>FD</sup> and GIRK4/4<sup>FD</sup> systems. The binding of ML297 or GAT1508 shifts the PIP<sub>2</sub>-binding site and increases *P-WT* interactions with the GIRK2 more so than GIRK4 WT subunits. The interaction between GAT1508 and the FD-mutated subunits decreases the channel *P-FD* interaction in both GIRK2 and GIRK4 heteromeric channels. *C*, average snapshots of PIP<sub>2</sub> interacting with GIRK2/GIRK4 Tyr-76/71 residues in the channel slide helix region with ML297 (*top*) and GAT1508 (*bottom*) binding in GIRK2/2<sup>FD</sup> (*left panels*) and GIRK4/4<sup>FD</sup> (*right panels*). PCA suggests large conformational changes induced by GAT1508 binding in GIRK2<sup>FD</sup> or ML297 binding in GIRK2<sup>FD</sup> and GIRK4<sup>FD</sup>. A strong H-bond interaction is formed between Tyr residue in the slide helix of FD-mutated subunit and P4/5 of PIP<sub>2</sub>, which can position the PIP<sub>2</sub> head group toward the junction of the M2 and TM-CTD (where CTD is cytoplasmic domain) linker and induce the increase in channel *P-WT* interactions. However, GAT1508 binding around the M2 helix of GIRK4/4<sup>FD</sup> results in loss of the H-bond interaction between GIRK4<sup>FD</sup>(Tyr-71) and PIP<sub>2</sub> and failure to position the head group for optimal interactions. *D*, minimum distance between the O atom of Tyr-76/71 in the FD-mutated subunits and P4,5-PIP<sub>2</sub>. *E*, sequence alignment of the GIRK channel Slide helix region. The key residue interactions proposed by the simulations for the GAT1508-induced changes in GIRK activation are highlighted. As polar residues, both Ser and Tyr could form H-bond interactions with PIP<sub>2</sub>.

GAT1508 and ML297 on the atrial optical action potential duration (APD) in an isolated Langendorff mouse heart preparation (52, 53). Fig. 10, *A* and *D*, shows fluorescence pictures of the right atria showing the superior vena cava, the right atrial appendage, and the stimulation electrode. In Fig. 10*B*, under control conditions, the APD at 70% repolarization (APD<sub>70</sub>) map of the stimulated right atrium had an average duration of 23.9 ms. Ten minutes after 2.4 μM ML297 was introduced through the perfusate (Fig. 10*C*), the APD<sub>70</sub> shortened dramatically, to an average of 16 ms, secondary to the activation of GIRK1/4 by ML297. Fig. 10*E* shows under control conditions that the average APD<sub>70</sub> was 21.8 ms, and 10 min after 2.4 μM

GAT1508 was introduced through the perfusate (Fig. 10*F*), the average APD<sub>70</sub> was 20.3 ms. Summary *bar graphs* show the significant decrease in APD by ML297 (Fig. 10*G*, *left panel*), unlike GAT1508 that did not shorten the APD (Fig. 10*G*, *right panel*).

We next compared the effects of the two compounds on the cardiac hERG channel expressed in *Xenopus* oocytes, a common target that many ligands are screened against to assess cardiac toxicity. Concentrations of GAT1508 up to 50 μM did not affect hERG channel currents, whereas 5 μM ML297 caused a significant block and 10 μM terfenadine produced a complete block of these currents (Fig. S8, *A–D*).



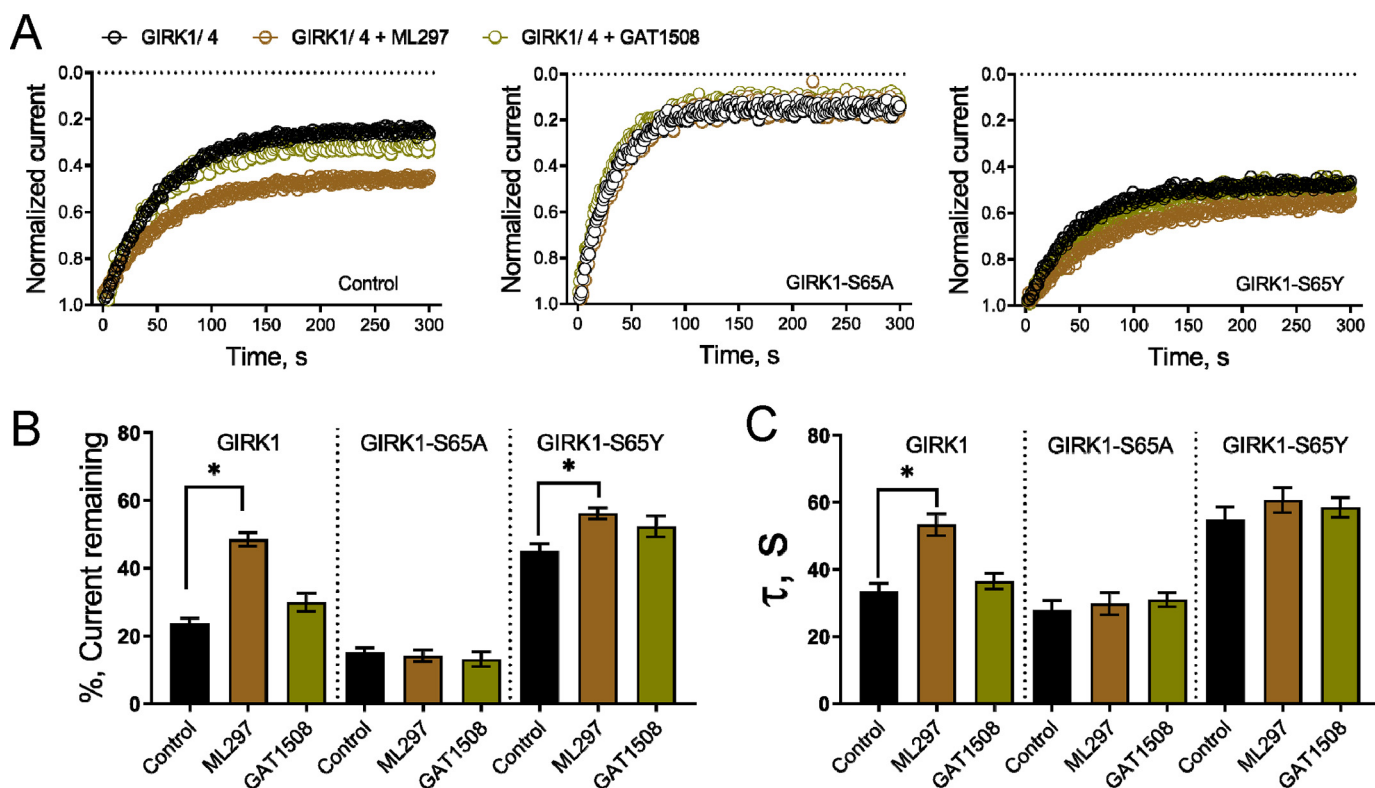


**Figure 9. GIRK1 subunit Slide helix residue Ser-65 is required for the drug-induced enhancement of GIRK activity.** Data are currents recorded from HEK293 cells using patch-clamp in the whole-cell mode and are shown as means  $\pm$  S.E. for 5–6 cells per group. Statistical significance was calculated using unpaired *t* tests. \*,  $p < 0.01$ . ML297 and GAT1508 were used at 10  $\mu\text{M}$ . *A*, left, representative plots of normalized current magnitude against time show that GIRK1/4 channel current decreases in response to light-activated metabolism of PIP<sub>2</sub> by the phosphatase 5-ptase<sub>OCRL</sub> (control, black open circles). The decrease in current is reduced when GIRK1/4 channels are studied in the presence of ML297 (brown open circle) but not with GAT1508 (olive green open circle). Middle, channels containing GIRK1-S65A subunit currents are more sensitive to 5-ptase<sub>OCRL</sub> and are not protected by either compound. Right, in contrast, channels with GIRK1-S65Y subunits are more protected than WT. *B*, bar graph representing the mean increase in the percentage of GIRK1/4 channel current remaining following activation of 5-ptase<sub>OCRL</sub> in the absence (control) or presence of ML297 or GAT1508. *C*, 5-ptase<sub>OCRL</sub>-mediated decrease in GIRK1/4 current is characterized by mono-exponential fits in the presence and absence of the compound indicated. The bar graph shows the mean  $\tau$  of current inhibition is increased when WT channels are fitted with ML297 but not GAT1508. This effect is decreased when GIRK1-S65A subunits are expressed. Channels with GIRK1-S65Y subunits have an increased  $\tau$  of current inhibition that is not statistically increased with ML297 or GAT1508.

#### GAT1508 activates GIRK1/2 channels and at subactivating concentrations potentiates baclofen-induced GIRK activation in basolateral amygdala brain slices

Next, we employed a whole-cell patch-clamp recording in acute brain slices to examine the effect of GAT1508. We utilized brain slices that included the BLA, a limbic structure that has been extensively described to coordinate the acquisition and expression of fear memories (54, 55). In the rat amygdala, GIRK mRNA expression reveals abundance of GIRK1, GIRK2, and GIRK3, but not GIRK4 transcripts (56). We observed that perfusion of 10  $\mu\text{M}$  GAT1508 did not produce responses in recordings of BLA neurons at  $-50$  mV, but 30  $\mu\text{M}$  GAT1508 produced significant outward current (ligand effect  $F_{2,16} = 10.1$ ,  $p = 0.0013$ , ANOVA, Fig. 11, *A* and *B*). These data further support that GAT1508 functions as a GIRK1/2 activator. Next, we examined the response of BLA neurons to baclofen, a GABA<sub>B</sub>-receptor agonist that induces GIRK-mediated potassium currents. Compared with baseline, a 100-ms puff of 100  $\mu\text{M}$  baclofen via a glass pipette tip induced a significant outward current (Tukey's post hoc test,  $p < 0.05$ , see Fig. 11, *C* and *D*, black trace and bars). In the same cells, a 10-min perfusion of 10  $\mu\text{M}$  GAT1508 significantly potentiated baclofen-induced current without affecting baseline currents recorded prior to

baclofen application (treatment effect  $F_{5,40} = 25.8$ ,  $p < 0.0001$ , ANOVA, Fig. 11, *C* and *D*, green trace and bars). Finally, antagonism of GIRK currents by 3 mM Ba<sup>2+</sup> blocked significant current responses (Fig. 11, *C* and *D*, gray trace and bars) suggesting that the baclofen response and the GAT1508 potentiation of the baclofen response are mediated by Ba<sup>2+</sup>-sensitive GIRK activity. GAT1508-mediated enhancement of GIRK currents at 10  $\mu\text{M}$ , a concentration that does not produce agonist activity, suggests that the compound functions synergistically with G-protein activation mechanisms (53), reminiscent of the action of a positive allosteric modulator (PAM) of a G-protein-coupled receptor.

#### Selective activation of GIRK1/2 channels facilitates fear extinction

Our slice electrophysiology data suggest that as an agonist and a "PAM," GAT1508 increases the GIRK-mediated inhibitory tone in the BLA. Because the BLA together with the central nucleus of the amygdala are essential structures in the neurocircuitry underlying fear conditions (57–65), we tested whether systemic treatment with different concentrations of GAT1508 and ML297 modulates fear memories in a Pavlovian conditioning fear paradigm. Rats treated with either GAT1508 (10 or 30

## A GIRK-specific activator in conditioned fear extinction

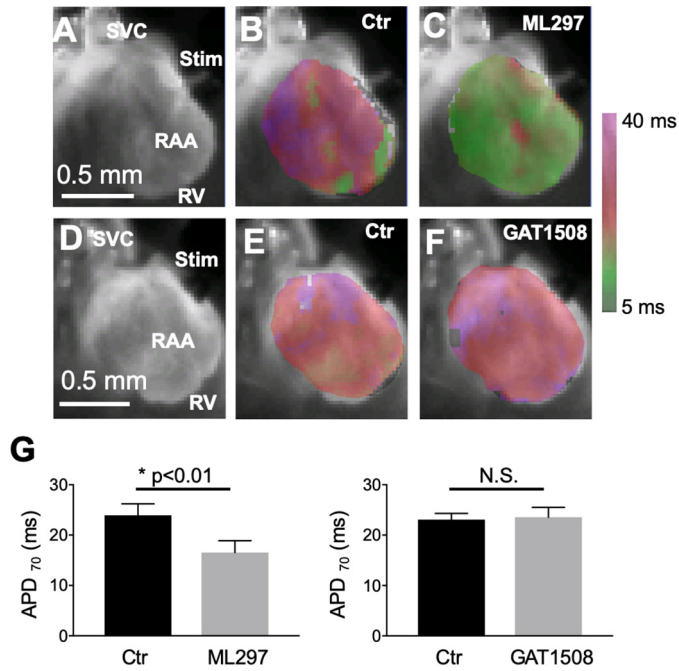


**Figure 10. Optical mapping of atrial electrical propagation in the isolated Langendorff-perfused mouse heart.** *A*, and *D*, fluorescence images of the mapped field. SVC, superior vena cava; RAA, right atrial appendage; RV, right ventricle; Stim, bipolar stimulation electrode. *B*, and *E*, APD<sub>70</sub> maps at 10 Hz stimulation in control. *C* and *F*, APD<sub>70</sub> maps at 10 Hz stimulation 10 min after perfusion with 2.4 μM ML297 and GAT1508, respectively. *G*, quantification of APD<sub>70</sub>, where ML297 at 2× IC<sub>50</sub> significantly shortened the duration from 23.93 ± 2.28 ms to 16.53 ± 2.36 ms,  $n = 3$ ,  $p < 0.01$  (paired *t* test). GAT1508, at concentrations severalfold higher than its IC<sub>50</sub> for activation of GIRK1/2 did not affect the atrial APD, where the duration was 23.1 ± 1.21 ms in control and 23.57 ± 1.96 ms in the presence of the drug,  $p$  is not significant (N.S.) (paired *t* test).

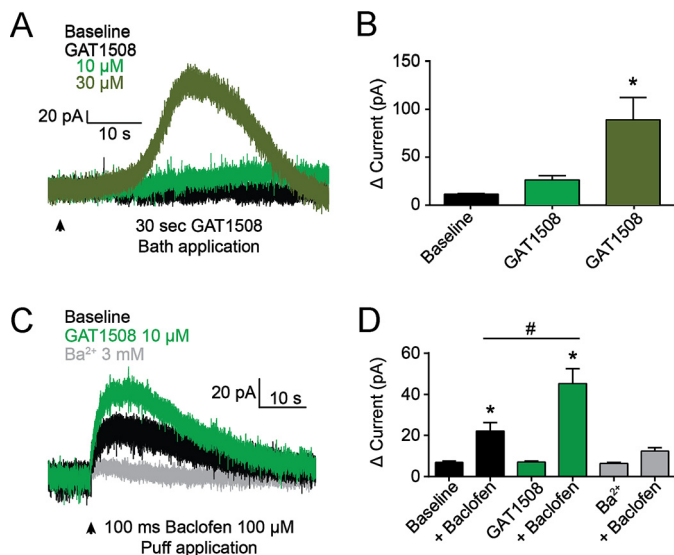


**Figure 11. GAT1508 demonstrates GIRK agonist and GIRK allosteric modulation in the BLA.** *A*, representative current responses from BLA neurons in response to 30 s of GAT1508 perfusion from a –50-mV holding potential. *B*, summary data depicting significant current response following 30 μM GAT1508. *C*, representative current responses from BLA neurons in response to 100 ms, 100 μM, baclofen administered via pressure micropipette. Responses to each condition were recorded from the same cells. *D*, summary data depicting significant current response to baclofen and significant potentiation of baclofen response by GAT1508 that was blocked by Ba<sup>2+</sup>. Symbols denote statistical significance by one-way ANOVA and Tukey's post hoc. \*,  $p < 0.05$  versus all other conditions; #,  $p < 0.05$  compares baclofen responses before and during GAT1508 treatment,  $n = 9$  cells.

mg/kg) or vehicle immediately after acquisition and 30 min prior to consolidation of fear memories (Fig. 12A) showed normal acquisition (tone effect,  $F_{4,96} = 576.4$ ,  $p < 0.0001$ ; see Fig. 12B) and consolidation of fear memories (tone effect,  $F_{4,96} = 8.1$ ,  $p < 0.0001$ ; see Fig. 12C). Additionally, all groups demonstrated significant extinction of fear memories, but animals treated with GAT1508 extinguished fear memories much faster than animals from the vehicle group (tone effect  $F_{19,456} = 41.9$ ,  $p < 0.0001$ , treatment effect  $F_{2,24} = 9.4$ ,  $p = 0.001$ , no interaction; see Fig. 12D). Dunnett's post hoc within each group test showed significant reduction of freezing behavior in the GAT1508 group by tone 4, whereas animals from the control group did not show significant reduction of freezing until tone 7 (Fig. 12D). Moreover, Sidak's between groups post hoc analysis confirmed significant differences between vehicle and GAT1508-treated groups ( $p = 0.008$  10 mg/kg GAT1508,  $p = 0.001$  30 mg/kg GAT1508; see Fig. 12D). Therefore, we conclude that systemic treatment with GAT1508 enhances extinction of fear memories.

Next, we assessed the effect of treatment with the nonselective compound ML297 on fear memories. Again, all three groups showed normal fear acquisition (treatment effect,  $p = 0.8$ , tone effect  $F_{4,120} = 650.5$ ,  $p < 0.0001$ ; see Fig. 12E). However, systemic pretreatment with ML297 at 30 mg/kg had no effect on consolidation of fear memories compared with the control group (treatment effect  $F_{1,15} = 0.09$ ,  $p = 0.77$ ; see Fig. 12F). Moreover, ML297-treated animals also showed no significant differences in extinction of fear memories compared with controls (treatment effect  $F_{1,15} = 0.56$ ,  $p = 0.47$ , tone effect  $F_{19,285} = 19.6$ ,  $p < 0.0001$ ). Dunnett's within group post hoc analysis revealed the reduction of freezing overtime by tone 6 in both groups of animals ( $p < 0.05$ , Fig. 12G). Pretreatment of ML297 at higher concentrations (60 mg/kg) did show significant reductions in consolidation and extinction of fear memories (Fig. 12, F–G), consistent with the *in vitro* findings suggesting it is less effective than GAT1508. Additionally, we also tested the effect of 30 and 60 mg/kg ML297 on motor activity using the open field (OF) test. The total distance traveled in the open arena and mean speed 30 min after ML297 treatment were comparable with the vehicle group (Fig. S9, A and B). Thus, the nonselective ML297 did not have the same effects of enhancing fear extinction like the GIRK1/2 GAT-selective compounds at comparable concentrations. In summary, the results of fear-conditioning experiments suggest that compounds selective to GIRK1/2 enhance extinction of fear memories.

### Selective activation of GIRK1/2 channels does not broadly affect behavioral, cognitive or motor functions

Next, we tested the effects of treatment with various doses of GAT1508 (10 and 30 mg/kg) on cognition, anxiety, and motor function using a battery of behavioral tests. First, in the elevated plus maze (EPM), animals treated with GAT1508 demonstrated a trend toward an increase of time spent on the open arm (from 30.6 ± 4.4 in vehicle group to 48.7 ± 8.3 s in 30 mg/kg of GAT1508 group; see Fig. S10A). In the light-dark box test, no difference in time spent in the light compartment was observed between vehicle and GAT1508-treated groups (Fig.

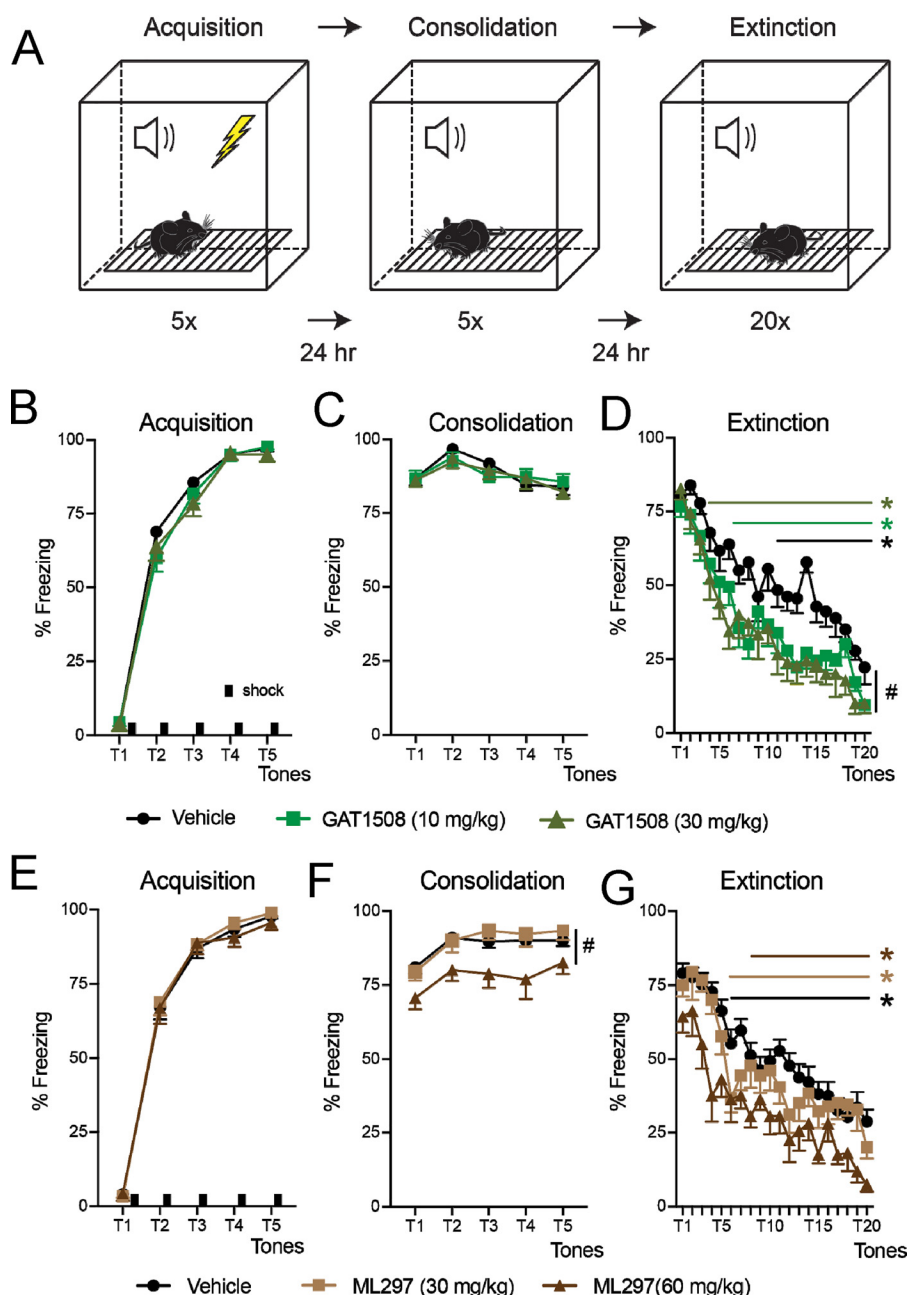


**Figure 12. Systemic pretreatment with GIRK1/2 allosteric modulators enhanced extinction of fear memories.** *A*, schematic diagram of the cue-induced fear-conditioning procedure (see under “Experimental procedures” for details). *B*, all groups of animals that had tone/shock pairings showed normal cue-induced fear acquisition. Animals were injected with vehicle (black solid circle) or GAT1508 at 10 mg/kg (green square), or 30 mg/kg (olive green triangle). *C*, pretreatment with GAT1508 had no effects on consolidation of fear memories. *D*, animals injected with either 10 or 30 mg/kg of GAT1508 showed significantly faster fear extinction compared with vehicle control rats. *E–G*, pretreatment with ML297 ( $n$ ; 30 mg/kg, light brown squares) did not affect acquisition (*E*) and consolidation (*F*) or extinction (*G*) of fear memories, while higher concentrations did (60 mg/kg, dark brown triangles). \*,  $p < 0.05$ , ANOVA with Tukey’s post hoc within group analysis. #,  $p < 0.05$ , ANOVA with Sidak’s post hoc between groups analysis.  $n = 9$  in all groups.

S10B). In the OF test, the total distance traveled and the mean speed after GAT1508 treatment were comparable with the vehicle group (Fig. S10, C and D). In the social interaction (SI) test, all groups showed similar interaction time (Fig. S10E). In the rotarod test, we also observed similar latency to fall between the vehicle and GAT1508-treated groups (Fig. S10F). Next, in the novel object recognition test, the discrimination index was also similar between the three groups, which suggests that GAT1508 treatment did not affect the ability to discriminate between novel and familiar arms (Fig. S10, G and H). Collectively,

our findings confirm that treatment with various doses of GAT1508 had no acute side effects on cognitive and motor functions.

### Discussion

We have produced a fully brain-specific activator for GIRK1/2 heteromers, GAT1508, that not only does not activate cardiac channels (GIRK1/4) but shows greater potency and efficacy than previous GIRK channel activators. Pharmacological optimization yielded a bromothiophene substitution as the pri-



## A GIRK-specific activator in conditioned fear extinction

mary determinant of the optimal interactions. The GAT1508-binding subunit GIRK1 utilizes two key residues (Phe-137 and Asp-173 or “FD”) to bind/transduce the effect of this class of small molecule activators. These two residues are necessary and sufficient to reproduce small molecule binding and activation effects. Heteromeric models (brain, GIRK2/2<sup>FD</sup>; heart, GIRK4/4<sup>FD</sup>) revealed that the brain-binding site stabilizes the urea scaffold (Site II) with hydrophobic residues to allow the aromatic ends of the small molecule in key  $\pi$  interactions. On one end (Site I) the bromothiophene engages in a network of  $\pi$  interactions through Phe residues to connect to the essential Phe residue in the pore helix (Phe-137 in GIRK1 and Phe-148 in GIRK2<sup>FD</sup>). On the other end, a benzene ring (Site IV) forms  $\pi$ -stacking interactions with another Phe residue (Phe-175 in GIRK1 and Phe-186 in GIRK2) to allow a neighboring Tyr residue (Tyr-91 in GIRK1 and Tyr-102 in GIRK2) to switch interaction partners from the first essential pore helix Phe to the second essential M2 helix Asp (Asp-173 in GIRK1, Asp-184 in GIRK2<sup>FD</sup>). These key interaction changes have allosteric consequences through the Slide helix and possibly the N terminus to enhance channel interactions with PIP<sub>2</sub> and cause opening of the channel gates.

The discovery of GAT1508, the first GIRK channel single subtype-specific activator for GIRK1/2 heteromers, overcomes the cardiac side effects of nonselective GIRK activators, as evidenced by the lack of a decrease in the atrial action potential duration in an isolated heart preparation, the lack of effect on hERG currents, or the lack of effects in heart rate and blood pressure in freely-moving animals. Because GIRK2 expression is restricted to the nervous system and GAT1508 fails to strengthen channel-PIP<sub>2</sub> interactions and activate peripheral GIRK1/4 channels, its effects would be expected to also be restricted to neuronal tissues. Detailed studies in adult rodent brains have suggested co-expression of the GIRK1/2 subunits in multiple brain regions, including the olfactory bulb, neocortex, hippocampus, cerebellum, thalamus, hypothalamus, and amygdala (34). Given this widespread pattern of expression, we decided to explore the effects of GAT1508 in the amygdala and in fear-conditioning paradigms, where the role of the physiological relevance and therapeutic potential of GIRK1/2 have not been studied in depth. Prior work from a decade ago suggested that the anxiolytic actions of the neuropeptide Y could be due to activation of GIRK currents that inhibited excitability in the lateral amygdala (66). Prior literature suggested that baclofen was efficacious in post-traumatic stress disorder by opening of GIRK channels through GABA<sub>B</sub> receptors (67). This prompted us to examine the effectiveness of baclofen in activating GIRK currents in brain slices of the basolateral amygdala. Indeed, not only could baclofen induce Ba<sup>2+</sup>-sensitive currents but so could sufficient concentrations of GAT1508. Interestingly, at lower concentrations of GAT1508, insufficient to produce significant GIRK activation, the baclofen responses were significantly potentiated, suggesting synergism in the allosteric effects of GAT1508 and G $\beta$  $\gamma$  in strengthening channel-PIP<sub>2</sub> interactions (53). These results further prompted us to examine the effectiveness of GAT1508 in fear extinction paradigms that serve as models of post-traumatic stress disorder.

Our positive results offer validation for both the physiological relevance and the therapeutic potential of GIRK1/2 as a drug target for post-traumatic stress disorder. The wide expression of GIRK1/2 in the brain begged the question of whether side effects could become limiting if GAT1508 were to be pursued as a candidate drug. The general positive results anticipated from GIRK channel activation in the brain (7) without cardiac side effects, as well as our negative results in rat behavioral tests modeling anxiety, memory, and social interaction with no additional obvious sedative or other overt behaviors, suggest that GAT1508 ought to be pursued further. Discovery of GAT1508 has opened a new therapeutic line of research for post-traumatic stress disorder and other fear-related neuropsychiatric disorders, which currently afflict millions of patients and are estimated to cost billions of dollars with very limited positive outcomes through existing pharmacotherapies.

### Experimental procedures

Animal experiments were approved by the Institutional Animal Care and Use Committees at Northeastern University, Boston, Indiana University at Indianapolis, and University of South Florida, Tampa.

### Chemistry

All commercial chemicals and solvents were purchased from standard commercial sources as reagent grade and, unless otherwise specified, were used without further purification. A Biotage Initiator microwave system was used for the synthesis. Reaction progress was monitored by thin-layer chromatography (TLC), using commercially prepared Silica Gel 60 F254 glass plates. Compounds were visualized under ultraviolet (UV) light or by staining with iodine. Flash column chromatography was carried out on an autoflash purification unit, using prepacked columns from Reveleris, Biotage and Lunknova. Solvents used include hexanes and ethyl acetate. Characterization of compounds and their purity were established by a combination of HPLC, TLC, MS, and NMR analyses. NMR spectra were recorded in DMSO-*d*<sub>6</sub>, on an NMR spectrometer (<sup>1</sup>H NMR at 500 MHz). Chemical shifts were recorded in parts per million ( $\delta$ ) relative to tetramethylsilane (0.00 ppm) or solvent peaks as the internal reference. Multiplicities were indicated as br (broadened), s (singlet), d (doublet), t (triplet), q (quartet), quin (quintet), and m (multiplet). Coupling constants (*J*) were reported in hertz (Hz). All test compounds were greater than 95% pure, as determined by LC-MS analysis performed with a dual-wavelength UV-visible detector and quadrupole mass spectrometer. The details of the general procedures used to synthesize the asymmetric urea ligands and their characterizations are shown in the [supporting information](#).

### Chemicals for electrophysiology

diC8-PIP<sub>2</sub> was purchased from Echelon, and terfenadine was from Sigma. ML297 and all GAT compounds were synthesized in-house as described above, maintained as 10 mM stock solutions in DMSO, and were diluted to concentrations between 10  $\mu$ M and 1 nM using the high K<sup>+</sup> buffer for electrophysiology experiments.

### Molecular biology

For *Xenopus* oocyte expression, human GIRK1 and human GIRK4 cDNAs were subcloned into pGEMHE (68). For mammalian expression, human GIRK1 and human GIRK4 cDNAs were subcloned into pcDNA3 and pcDNA3.1/V5-His B, respectively (Invitrogen). Mouse GIRK2 cDNA was subcloned in the dual-function vector, pXoom (69). Point mutations were introduced using a standard *Pfu*-based mutagenesis technique according to the QuikChange protocol (Agilent). Mutations were verified by sequencing.

### Functional assays

We used heterologous expression and electrophysiological studies of ion channels in two cell systems: freshly-isolated *Xenopus* oocytes and the HEK293 cell line. Some of the advantages of each of these two cellular systems over the other are mentioned below as justification for their use. Oocytes and the ease of recording made them the preferred system for screening compounds and characterizing mutants. Similarly, diC8-PIP<sub>2</sub> dose-response curves were easiest to pursue in inside-out macropatches from *Xenopus* oocytes. In contrast, HEK293 cells were the preferred cell system in assessing drug-induced changes in channel-PIP<sub>2</sub> interactions using the light-activated phosphatase system. Similarly, for accurate assessment of pharmacological parameters (e.g. potency and efficacy), whole-cell patch-clamp of HEK293 cells was the preferred method of choice.

*X. laevis* oocyte expression—Plasmid DNAs of GIRK channel subunits were linearized prior to *in vitro* transcription. Capped RNAs were transcribed using mMMESSAGE mMACHINE T7 transcription kit (Thermo Fisher Scientific). *Xenopus* oocytes were surgically extracted, dissociated, and defolliculated by collagenase treatment and microinjected with 50 nl of a water solution containing 1 ng of each GIRK subunit RNA. For TEVC experiments, oocytes were kept 2 days at 17 °C before recording, whereas for the NPo experiments oocytes were incubated for up to 4 days at 17 °C.

*Two-electrode voltage-clamp and data analysis*—Whole-oocyte currents were measured by TEVC with GeneClamp 500 (Molecular Devices) or TEC-03X (NPI) amplifiers. Electrodes were pulled using a Flaming-Brown micropipette puller (Sutter Instruments) and were filled with 3 M KCl in 1.5% (w/v) agarose to give resistances between 0.5 and 1.0 MΩ. The oocytes were bathed in ND96 recording solution comprising (in mM): KCl 2, NaCl 96, MgCl<sub>2</sub> 1, and HEPES 5, buffered to pH 7.4 with KOH. Where indicated, GIRK channel currents were assessed in a high-K<sup>+</sup> recording solution comprising (in mM): KCl 96, NaCl 2, MgCl<sub>2</sub> 1, and HEPES 5, buffered to pH 7.4 with KOH. Currents were digitized using a USB interface (National Instruments) and recorded using WinWCP software (University of Strathclyde). To study GIRK channels, oocytes were held at 0 mV, and currents were assessed by 100-ms ramps from −80 to +80 mV that were repeated every second. The effect of the reagents was determined at −80 mV and then the channels were blocked by 5 mM BaCl<sub>2</sub>. Block was expressed as the percent-current block normalized to the maximum current.

Between 8 and 12 oocytes from different *Xenopus* frogs were studied per experiment.

*Oocyte macropatch studies*—Macropatch GIRK channel activity was recorded from devitellinized oocytes under the inside-out mode of standard patch-clamp methods using an AM2400 patch-clamp amplifier (A-M Systems). Currents were digitized using a USB-interface (National Instruments) and WinEDR (University of Strathclyde) data acquisition software. Electrodes were fabricated using Kimax glass (WPI) and had a resistance of 0.5–1 MΩ when filled with an electrode solution containing (in mM): 96 KCl, 1 MgCl<sub>2</sub>, and 5 HEPES, pH 7.4. Oocytes were bathed with a solution comprising (in mM): 96 KCl, 5 EGTA, 1 MgATP, and 10 HEPES, pH 7.4. Current amplitudes were measured at −80 mV with a sampling rate of 10 kHz. Data were analyzed using WinEDR and Clampfit software (Molecular Devices).

*Culture of HEK293 cells*—HEK293-T cells were obtained from the ATCC and maintained in Dulbecco's modified Eagle's medium supplemented with 10% fetal bovine serum and 1% penicillin and streptomycin (HyClone). For patch-clamp studies, cells were seeded on glass coverslips and transfected 24 h later using a polyethyleneimine solution (1 mg/ml) at a ratio of 8 μl per μg of DNA. To study GIRK currents, cells were transfected with 0.75 μg each of plasmids encoding GIRK1, GIRK2, or GIRK4 as indicated. In the optogenetic experiments, cells were co-transfected with plasmids encoding CRY2–5-ptase<sub>OCRL</sub> and CIBN–CAAX (where A is any aliphatic amino acid and X is any amino acid), as described previously (64). 5-ptase<sub>OCRL</sub> and CIBN–CAAX were the kind gifts from the De Camilli lab (Yale University, New Haven, CT). All experiments were performed at room temperature 24–36 h post-transfection.

*Patch-clamp recording*—Whole-cell currents were recorded with an Axopatch<sup>TM</sup> 200B amplifier (Molecular Devices) controlled via a USB-interface (National Instruments) using WinWCP software (University of Strathclyde). Currents were acquired through a low-pass Bessel filter at 2 kHz and were digitized at 10 kHz. Patch pipettes were fabricated from borosilicate glass (Clark), using a vertical puller (Narishige) and had a resistance of 2.5–4 MΩ when filled with an intracellular buffer comprising: 140 mM KCl, 2 mM MgCl<sub>2</sub>, 1 mM EGTA, 5 mM Na<sub>2</sub>ATP, 0.1 mM Na<sub>2</sub>GTP, and 5 mM HEPES, pH 7.2. Cells for study were selected based on GFP expression using an epifluorescence microscope (Nikon). To study the activity of GIRK channels, cells were held at 0 mV, and currents were assessed by ramps from −80 to +80 mV that were repeated at 1 Hz. Cells were perfused via a multichannel gravity-driven perfusion manifold with a physiological buffer comprising: 135 mM NaCl, 5 mM KCl, 1.2 mM MgCl<sub>2</sub>, 1.5 mM CaCl<sub>2</sub>, 8 mM glucose, and 10 mM HEPES, pH 7.4, and then quickly transitioning to a high-K<sup>+</sup> buffer comprising 5 mM NaCl, 135 mM KCl, 1.2 mM MgCl<sub>2</sub>, 1.5 mM CaCl<sub>2</sub>, 8 mM glucose, and 10 mM HEPES, pH 7.4. The barium-sensitive component of the current, observed when cells were perfused with the high-K<sup>+</sup> buffer, was analyzed and determined by perfusing 5 mM BaCl<sub>2</sub> in the high-K<sup>+</sup> buffer at the end of each experiment. HEK293 cells had a mean whole-cell capacitance of 10 ± 1 picofarads; series resistance was typically <10 MΩ, and the voltage-error of <3 mV was not adjusted.

## A GIRK-specific activator in conditioned fear extinction

**Light-activated phosphatase system**—We used a light-activated phosphatase system to dephosphorylate PIP<sub>2</sub> that is composed of two fusion proteins: CRY2–5-ptase<sub>OCRL</sub> contains the photolyase domain of cryptochrome 2 (CRY2) and the inositol 5-phosphatase domain of the Lowe oculocerebrorenal syndrome protein (OCRL), and the CIBN–CAAX contains the CRY2-binding domain (CIBN) and a C-terminal CAAX box for plasma membrane targeting. When CRY2–5-ptase<sub>OCRL</sub> and CIBN–CAAX fusion proteins are co-expressed and exposed to blue light between 458 and 488 nm, the 5-ptase is localized to the plasma membrane, where it dephosphorylates PIP<sub>2</sub>. The utility of this system to study the PIP<sub>2</sub> dependence of ion channel activity was demonstrated by the Hille and De Camilli labs (51). The 5-ptase<sub>OCRL</sub> system was activated using a 460-nm LED (Luminus) that was focused on the cells through the objective lens of an inverted microscope (Nikon).

**Electrophysiological recordings from brain slices containing BLA neurons**—Electrophysiology was performed using 150–200-g male Sprague-Dawley rats (Harlan/Envigo, Indianapolis, IN). Rats were group-housed in plastic cages in standard housing conditions with *ad libitum* access to food and water with 12:12 light/dark cycle (lights on at 07:00 h). All experiments were conducted in accordance with the Guide for the Care and Use of Laboratory Animals (Institute for Laboratory Animal Research, National Academies Press) and the guidelines of the IUPUI Institutional Animal Care and Use Committee. Rats were anesthetized with isoflurane and immediately decapitated. Brains were then rapidly removed, placed in ice-cold oxygenated artificial cerebrospinal fluid solution (ACSF), and coronal slices (350 μm) were prepared containing the amygdala. Slices were incubated at 31 °C for 30 min and then returned to room temperature until recording. ACSF solution contains the following (in mM): 130 NaCl; 3.5 KCl; 1.1 KH<sub>2</sub>PO<sub>4</sub>; 1.3 MgCl<sub>2</sub>; 2.5 CaCl<sub>2</sub>; 30 NaHCO<sub>3</sub>; 10 glucose, 315 mosM, pH 7.4. Cells were identified for recording at ×40 magnification using Scientifica Slicescope microscope under differential interference contrast illumination (Scientifica, Uckfield, UK). ACSF was warmed to 30 °C and perfused at a rate of 2–3 ml/min during recordings. Compounds were added to ACSF at desired concentrations. Whole-cell patch-clamp recordings were obtained using standard techniques. Borosilicate glass electrodes (WPI, Sarasota, FL) (resistance 3–6 MΩ) were prepared and used for both recording and baclofen application. Recording internal solution contains the following (in mM): 140 K-gluconate; 2 KCl; 3 MgCl<sub>2</sub>; 10 HEPES; 5 phosphocreatinine; 2 K-ATP; 0.2 Na-GTP, 290 mosM, pH 7.4. In voltage-clamp mode, the cell was adjusted to –50 mV at the beginning of all experiments, and 5-min stable baseline was established before treatment. A Picospritzer II (Parker Hannifin, Hollis, NH) was utilized for local application of 100 μM of the GABA<sub>B</sub> agonist baclofen in ACSF to activate GIRKs. Baseline and baclofen-induced currents were averaged from three responses per cell and analyzed using ClampFit software (Molecular Devices, San Jose, CA). Ba<sup>2+</sup> depolarized resting potential suggesting that BLA GIRK channels contribute to resting membrane potential. Several control cells were subjected to baclofen at 2-min intervals for 30 min, and consistent responses were observed, thus ruling out time-dependent effects.

**Optical mapping studies in isolated hearts**—Isolated hearts of C57BL/6 mice, 4–6 months of age, were retrogradely perfused with Tyrode's solution in the Langendorff mode. The preparations were maintained at 37 °C, stained with a bolus of a voltage-sensitive dye (0.25 ml, 10 μM di-4-ANEPPS 3-(4-(2-(6-(Dibutylamino)naphthalen-2-yl)vinyl)pyridinium-1-yl)propane-1-sulfonate, Molecular Probes), and imaged with a CCD camera (RedShirt Imaging), 80 × 80 pixels, 85 μm per pixel, and 1000 frames/s (1). Excitation contraction uncoupling was achieved with 7 μM blebbistatin (Tocris Bioscience). A bipolar, silver tip stimulation electrode was used to pace the right atrium (2.5 pulses, 2× diastolic threshold) at 10 Hz using an AD Instrument stimulation platform. ML297 or GAT1508 at 2.4 μM were introduced into the perfusate. The action potential duration at 70% repolarization (APD<sub>70</sub>) was quantified, as we have previously reported 52, 53.

### Computational modeling

**Molecular docking**—To accurately reproduce the geometry of ML297 and the GAT molecules, we optimized their structures by Gaussian 03. Restrained electrostatic potential (RESP) charges were derived by calculated quantum mechanics (QM) charges and were used during docking and molecular dynamics simulation procedures (75–76). We used AutoDock 4.2 to dock ML297 and the GAT compounds to the GIRK2/GIRK2<sup>FD</sup> (from the crystal structure, PDB code 3SYA) and GIRK4/GIRK4<sup>FD</sup> heteromers, a homology model of which was constructed based on the GIRK2 crystal structure (PDB code 3SYA) by the MODELLER program. Although both the S148F and N184D mutations are required for ML297 activation, the Phe residue at position 148 is located in the pore helix and is unlikely to directly interact with ML297. Thus, the docking box (size: 22.5 × 22.5 × 30 Å) was set around Asp-184 of each of the two FD subunits. During docking, ML297 was treated as a flexible molecule, whereas the channel subunits were treated as rigid bodies. We obtained 270,000 docking conformations each for the GIRK2 and GIRK2/2<sup>FD</sup> models. By empirical free-energy scoring, we selected the 100 top docking configurations. The most favorable binding configuration with the lowest binding energy was selected for further analysis. A second set of docking calculations was also performed using the induced-fit docking protocol in the Schrodinger 2017 version 4 package. During docking, ligands and subunits were parameterized with the OPLS3 force field. Eighty initial poses were generated and carried into the refinement stage. An implicit membrane was used in the protein refinement stage. The final redocking stage used the Glide XP docking protocol and scoring (77–80).

**MD simulation experiments GROMACS**—The GIRK2/GIRK2<sup>FD</sup> and GIRK4/GIRK4<sup>FD</sup> channel in the presence or absence of ML297 and GAT1508 docked to the “FD”-containing subunits were subjected to MD simulations with four PIP<sub>2</sub> molecules. GROMACS version 4.5 was used to conduct simulations, applying the GROMOS96 53a6 force field. Topology files and charges for the atoms of PIP<sub>2</sub> and the compounds were calculated using the PRODRG web server, as described in previous work (70–72). The channel–drug–PIP<sub>2</sub> structures were immersed in an explicit POPC, POPE, POPS, and cholesterol bilayer (25:5:5:1), using the CHARMM GUI membrane package



and solvated with simple point charge (SPC) water molecules in 150 mM KCl. To mimic the activated state, we applied a constant depolarizing electric field of  $-0.128 \text{ V}\cdot\text{nm}^{-1}$ . Energy minimization was performed, followed by a 800-ps position-restrained (1000 kJ/mol/nm<sup>2</sup>) MD run. Subsequently, the six systems (GIRK2/2<sup>FD</sup>, GIRK4/4<sup>FD</sup>, alone and each of ML297 and GAT1508) we ran were subjected to 100-ns MD simulations. The SIMULAID program was used to analyze/cluster structures and to calculate interaction networks, including hydrogen bonds, salt bridges, and hydrophobic contacts.

**Amber**—MD simulation experiments were also carried out using the Amber package. The GIRK2/2<sup>FD</sup> and GIRK4/4<sup>FD</sup> channels in the presence or absence of ML297 or GAT1508 in the FD-containing subunits were subjected to MD simulations with four PIP<sub>2</sub> molecules. Amber18 was used to conduct simulations, applying the Amber ff14sb and Lipid14 force fields. Ligand geometries and charges were generated at the b3lyp/cc-pvtz level using Gaussian 16. Topology files were created using the CHARMM GUI Membrane builder web server. The channel–ligand–PIP<sub>2</sub> structures were immersed in an explicit POPC, POPE, POPS, and cholesterol bilayer at a ratio of 25:5:5:1, respectively. Systems were solvated in a TIP3 water model. Resulting models were neutralized with KCl with an additional 150 mM KCl added to the system. 10,000 steps of energy minimization were performed on each system. After the first 5000 steps of steepest descent, a conjugate gradient was used. Four heating steps were used to bring the system to 300 K. In the initial heating set, the system was heated to 100 K over the course of 2 ns with a 1-fs time step. The protein was held under a 20.0 kJ/mol/nm<sup>2</sup> constraint. The membrane was held under a 10.0 kJ/mol/nm<sup>2</sup> constraint. This step was followed by an additional 2 ns where the temperature was raised from 100 to 300 K under the same conditions as the initial heating step. In the third phase, the constraints were relaxed to 10.0 kJ/mol/nm<sup>2</sup>. In the final phase, the restraints were finally relaxed to 1.0 kJ/mol/nm<sup>2</sup>. The production phases for these simulations consisted of 105 ns with a 3-fs time step. Simulations were run in triplicate on the systems containing a compound. Subsequently, the six systems (GIRK2/2<sup>FD</sup>, GIRK4/4<sup>FD</sup>, alone and with ML297, and GAT1508) were analyzed with the SIMULAID and CPPTRAJ programs to calculate interatomic distances, hydrogen bonds, salt bridges, and hydrophobic contacts.

All the computational results were generated based on a 100-ns MD run by GROMACS. To enhance the amount of sampling of ligand binding and for further mechanistic studies, three MD run replicas were generated using AMBER and were included in assessing key-residue and channel–PIP<sub>2</sub> interactions.

### Behavioral studies

**Cued fear conditioning test**—On day 1, animals were habituated to the sound-attenuating fear-conditioning chamber (Kinder Scientific, Poway, CA) for 10 min. Between each animal, the chamber was cleaned with 70% ethanol. On day 2, acquisition of fear was achieved by placing rats back into the chamber for a 120-s acclimation period and then five pairings (120-s inter-trial interval) of the conditioned stimulus (CS; 20 s, 80 db) followed immediately by the unconditioned shock stim-

ulus (500 ms, 0.8-mA foot shock). On day 3, CS consolidation was assessed by placing the rats back into the chamber with a 120-s acclimation period followed by five presentations of the CS only (20 s, 80 db) with 120-s inter-trial intervals. On day 4, extinction was assessed by presenting a 120-s acclimation period followed by 20 trials of the CS (20 s, 80 db) with 120-s inter-trial intervals. The same experimenter (S. D. F.) handled the rats during all sessions and was blinded to the treatment. All trials were digitally video-recorded. For this behavioral test and all others, blind scoring was aided by modification of video file names by A.I.M. Freezing behavior (no visible signs of movement) was scored by S. D. F. during the sound presentation and converted to percentage of total time.

**Open test (OF) test**—The OF apparatus is a Plexiglas open-topped chamber (91.5 × 91.5 × 30.5 cm), filmed by a ceiling-mounted CCD camera, and illuminated by a 25-watt red light bulb placed 2 m above the center of the chamber. One hour after vehicle or ligand treatment, rats were gently placed in the center and allowed to freely move for 5 min. The automated tracking system ANY-MAZE (ANY-MAZE, Stoelting Co., Wood Dale, IL) was utilized to measure total distance traveled and mean speed.

**Social interaction (SI) test**—The SI test was performed 5 min after the OF test in the same apparatus. The protocol used for the SI test has been described previously (65). In brief, the “experimental” rat and the “partner” rat were simultaneously placed into the chamber for a 5-min test. The “partner” rat was age-, sex-, and weight-matched to the experimental rat. All tests were video recorded and then manually scored using ODlog for Mac OS X version 2.6.1. Time spent by the experimental rat engaging in nonaggressive physical investigation of the partner rat is reported as social interaction time (in seconds). Investigation of the partner includes sniffing, climbing over and crawling under, mutual grooming, genital investigation, or following and walking around the partner.

**Novel object recognition test (NORT)**—The novel object recognition test was performed in an open-field box measuring 100 × 100 × 20 cm as described previously (66). Prior to testing, the rats were allowed to explore the box for 5 min per day for 3 consecutive days with no objects present. Testing consisted of two 2-min trials. During a familiarization trial, two identical objects (plastic cylinders 6 cm in diameter and 12 cm tall in white and red) were placed in two adjacent corners. The animal was then released against the center of the opposite wall with its back to the objects. This was done to prevent coercion to explore the objects. The animals were regarded to be exploring when they were facing, sniffing, or biting the object with nose and/or forepaws. Immediately after familiarization, the rats received intraperitoneal (i.p.) injections of vehicle or ligands and were returned to their home cage. After a waiting period of 3 h (Inter-trial-interval or ITI = 3 h), the rat was placed in the box again, and the test trial was performed. During this trial, a new object (plastic building block in yellow or green, 7 × 3.5 × 9 cm) replaced one of the familiar objects used in the familiarization trial. The times spent exploring each object during both trials was recorded manually by using a stopwatch. The box and the objects were cleaned with 70% ethanol between trials. Discrimination index (DI) was used to measure object recognition

## A GIRK-specific activator in conditioned fear extinction

and is calculated as the difference in time exploring the novel (TN) versus the familiar object (TF), then dividing this value by the total time spent exploring the two objects in the test trial.  $DI = TN - TF / TN + TF$ .

**Light-dark box**—The light-dark box test was performed using a cage  $52 \times 100 \times 39$  cm divided into two equal sections by an opening. One section is brightly illuminated, and the other section is dark. Animals were injected 30 min prior to testing with vehicle or ligand and then placed into the light side with immediate access to explore the entire cage. Time spent in the illuminated section was analyzed. The chamber was cleaned between each experiment.

**Rotarod tests**—Animals were habituated to the rotarod test for 5 consecutive days and tested on day 6. On the test day, animals were injected with vehicle or GAT1508 30 min prior to testing. Each day consisted of three trials separated by 1 min. A trial constituted animals being placed on an immobile rotarod that was then accelerated from 0 to 40 rotations/min. Trials lasted 120 s during which the rotarod accelerated at a rate of 0.33 rotations/s. Mechanical detection of the latency to fall was registered by Panlab RotaRod RS (Harvard Apparatus, Holliston, MA).

**Elevated plus maze (EPM)**—The EPM, as described previously (67), was performed in a black Plexiglas apparatus (Hamilton Kinder, San Diego, CA) that consists of two open arms and two closed arms each 50.17 cm long and 10.8 cm wide. The closed arms have walls that are 40.01 cm high. The entire apparatus is elevated 100 cm above the ground on a square aluminum base. For a testing period of 5 min, anxiety is estimated by the amount of time rats spend in the closed versus open arms. Test sessions were video recorded by ceiling-mounted cameras.

**Cardiovascular experiments**—Radio telemetry probes (catalog no. HD-S11, Data Sciences International, St. Paul, MN) were surgically implanted into the peritoneal cavity and sutured to the muscle wall to assess general motor activity and temperature. A pressure transducer was implanted into the femoral artery to assess cardiovascular responses (*i.e.* MAP and HR). Animals were injected with selected compounds following a 10-min baseline period, and data points were analyzed between 20 and 60 min after injection. This allowed us to investigate ligand effects without confounding effects of animal handling or the injection itself and to allow the ligand to cross the blood-brain barrier.

**Author contributions**—Y. X., L. C., A. I. M., L. D. P., D. G., S. D. F., E. T. D., Y. Y., T. K., S. G., S. F. N., A. S., D. E. L., and G. A. T. data curation; Y. X., A. I. M., L. D. P., and D. G. modeling; Y. X., L. C., A. I. M., L. D. P., D. G., S. F. N., A. S., D. E. L., and G. A. T. formal analysis; Y. X., L. C., A. I. M., L. D. P., D. G., S. F. N., A. S., D. E. L., and G. A. T. validation; Y. X., L. C., A. I. M., L. D. P., D. G., S. D. F., E. T. D., Y. Y., T. K., S. G., S. F. N., A. S., D. E. L., and G. A. T. investigation; Y. X., L. C., A. I. M., L. D. P., D. G., S. F. N., A. S., D. E. L., and G. A. T. visualization; Y. X., L. C., A. I. M., L. D. P., T. K., S. G., S. F. N., D. E. L., and G. A. T. methodology; Y. X., L. C., A. I. M., L. D. P., S. F. N., A. S., D. E. L., and G. A. T. writing-original draft; A. I. M., L. D. P., S. F. N., A. S., D. E. L., and G. A. T. conceptualization; A. I. M., S. F. N., A. S., D. E. L., and G. A. T. supervision; S. F. N., A. S., D. E. L., and G. A. T. resources; S. F. N., A. S., D. E. L., and G. A. T. funding acquisition; A. S., D. E. L., and G. A. T. project administration; D. E. L. writing-review and editing.

**Acknowledgments**—We are grateful to Heikki Vaananen for oocyte preparation and overall technical support. We also thank Dr. Pietro De Camilli for providing the light-activated phosphatase construct.

## References

1. Dascal, N., and Kahanovitch, U. (2015) The roles of  $G\beta\gamma$  and  $G\alpha$  in gating and regulation of GIRK channels. *Int. Rev. Neurobiol.* **123**, 27–85 [CrossRef Medline](#)
2. Doupnik, C. A. (2015) RGS redundancy and implications in GPCR-GIRK signaling. *Int. Rev. Neurobiol.* **123**, 87–116 [CrossRef Medline](#)
3. Glaaser, I. W., and Slesinger, P. A. (2015) Structural insights into GIRK channel function. *Int. Rev. Neurobiol.* **123**, 117–160 [CrossRef Medline](#)
4. Hibino, H., Inanobe, A., Furutani, K., Murakami, S., Findlay, I., and Kurachi, Y. (2010) Inwardly rectifying potassium channels: their structure, function, and physiological roles. *Physiol. Rev.* **90**, 291–366 [CrossRef Medline](#)
5. Logothetis, D. E., Mahajan, R., Adney, S. K., Ha, J., Kawano, T., Meng, X. Y., and Cui, M. (2015) Unifying mechanism of controlling Kir3 channel activity by G proteins and phosphoinositides. *Int. Rev. Neurobiol.* **123**, 1–26 [CrossRef Medline](#)
6. Lüscher, C., and Slesinger, P. A. (2010) Emerging roles for G protein-gated inwardly rectifying potassium (GIRK) channels in health and disease. *Nat. Rev. Neurosci.* **11**, 301–315 [CrossRef Medline](#)
7. Luján, R., Marron Fernandez de Velasco, E., Aguado, C., and Wickman, K. (2014) New insights into the therapeutic potential of GIRK channels. *Trends Neurosci.* **37**, 20–29 [CrossRef Medline](#)
8. Marron Fernandez de Velasco, E., McCall, N., and Wickman, K. (2015) GIRK channel plasticity and implications for drug addiction. *Int. Rev. Neurobiol.* **123**, 201–238 [CrossRef Medline](#)
9. Mayfield, J., Blednov, Y. A., and Harris, R. A. (2015) Behavioral and genetic evidence for GIRK channels in the CNS: role in physiology, pathophysiology, and drug addiction. *Int. Rev. Neurobiol.* **123**, 279–313 [CrossRef Medline](#)
10. Tipps, M. E., and Buck, K. J. (2015) GIRK Channels: a potential link between learning and addiction. *Int. Rev. Neurobiol.* **123**, 239–277 [CrossRef Medline](#)
11. Clapham, D. E., and Neer, E. J. (1997) G protein  $\beta\gamma$  subunits. *Annu. Rev. Pharmacol. Toxicol.* **37**, 167–203 [CrossRef Medline](#)
12. Logothetis, D. E., Kurachi, Y., Galper, J., Neer, E. J., and Clapham, D. E. (1987) The  $\beta\gamma$  subunits of GTP-binding proteins activate the muscarinic  $K^+$  channel in heart. *Nature* **325**, 321–326 [CrossRef Medline](#)
13. Reuveny, E., Slesinger, P. A., Inglese, J., Morales, J. M., Iñiguez-Lluhi, J. A., Lefkowitz, R. J., Bourne, H. R., Jan, Y. N., and Jan, L. Y. (1994) Activation of the cloned muscarinic potassium channel by G protein  $\beta\gamma$  subunits. *Nature* **370**, 143–146 [CrossRef Medline](#)
14. Huang, C. L., Feng, S., and Hilgemann, D. W. (1998) Direct activation of inward rectifier potassium channels by  $PIP_2$  and its stabilization by  $G\beta\gamma$ . *Nature* **391**, 803–806 [CrossRef Medline](#)
15. Logothetis, D. E., Petrou, V. I., Zhang, M., Mahajan, R., Meng, X. Y., Adney, S. K., Cui, M., and Baki, L. (2015) Phosphoinositide control of membrane protein function: a frontier led by studies on ion channels. *Annu. Rev. Physiol.* **77**, 81–104 [CrossRef Medline](#)
16. Mahajan, R., Ha, J., Zhang, M., Kawano, T., Kozasa, T., and Logothetis, D. E. (2013) A computational model predicts that  $G\beta\gamma$  acts at a cleft between channel subunits to activate GIRK1 channels. *Sci. Signal.* **6**, ra69 [CrossRef Medline](#)
17. Sui, J. L., Petit-Jacques, J., and Logothetis, D. E. (1998) Activation of the atrial KACH channel by the  $\beta\gamma$  subunits of G proteins or intracellular  $Na^+$  ions depends on the presence of phosphatidylinositol phosphates. *Proc. Natl. Acad. Sci. U.S.A.* **95**, 1307–1312 [CrossRef Medline](#)
18. Meng, X. Y., Zhang, H. X., Logothetis, D. E., and Cui, M. (2012) The molecular mechanism by which  $PIP_2$  opens the intracellular G-loop gate of a Kir3.1 channel. *Biophys. J.* **102**, 2049–2059 [CrossRef Medline](#)
19. Whorton, M. R., and MacKinnon, R. (2011) Crystal structure of the mammalian GIRK2  $K^+$  channel and gating regulation by G proteins,  $PIP_2$ , and sodium. *Cell* **147**, 199–208 [CrossRef Medline](#)

20. Whorton, M. R., and MacKinnon, R. (2013) X-ray structure of the mammalian GIRK2- $\beta\gamma$  G-protein complex. *Nature* **498**, 190–197 [CrossRef Medline](#)
21. Ho, I. H., and Murrell-Lagnado, R. D. (1999) Molecular determinants for sodium-dependent activation of G protein-gated K<sup>+</sup> channels. *J. Biol. Chem.* **274**, 8639–8648 [CrossRef Medline](#)
22. Ho, I. H., and Murrell-Lagnado, R. D. (1999) Molecular mechanism for sodium-dependent activation of G protein-gated K<sup>+</sup> channels. *J. Physiol.* **520**, 645–651 [CrossRef Medline](#)
23. Sui, J. L., Chan, K. W., and Logothetis, D. E. (1996) Na<sup>+</sup> activation of the muscarinic K<sup>+</sup> channel by a G-protein-independent mechanism. *J. Gen. Physiol.* **108**, 381–391 [CrossRef Medline](#)
24. Zhang, H., He, C., Yan, X., Mirshahi, T., and Logothetis, D. E. (1999) Activation of inwardly rectifying K<sup>+</sup> channels by distinct PtdIns(4,5)P<sub>2</sub> interactions. *Nat. Cell Biol.* **1**, 183–188 [CrossRef Medline](#)
25. Kobayashi, T., Ikeda, K., Kojima, H., Niki, H., Yano, R., Yoshioka, T., and Kumanishi, T. (1999) Ethanol opens G-protein-activated inwardly rectifying K<sup>+</sup> channels. *Nat. Neurosci.* **2**, 1091–1097 [CrossRef Medline](#)
26. Lewohl, J. M., Wilson, W. R., Mayfield, R. D., Brozowski, S. J., Morrisett, R. A., and Harris, R. A. (1999) G-protein-coupled inwardly rectifying potassium channels are targets of alcohol action. *Nat. Neurosci.* **2**, 1084–1090 [CrossRef Medline](#)
27. Weigl, L. G., and Schreibmayer, W. (2001) G protein-gated inwardly rectifying potassium channels are targets for volatile anesthetics. *Mol. Pharmacol.* **60**, 282–289 [CrossRef Medline](#)
28. Yamakura, T., Lewohl, J. M., and Harris, R. A. (2001) Differential effects of general anesthetics on G protein-coupled inwardly rectifying and other potassium channels. *Anesthesiology* **95**, 144–153 [CrossRef Medline](#)
29. Yow, T. T., Pera, E., Absalom, N., Heblinski, M., Johnston, G. A., Hanrahan, J. R., and Chebib, M. (2011) Naringin directly activates inwardly rectifying potassium channels at an overlapping binding site to tiapin-Q. *Br. J. Pharmacol.* **163**, 1017–1033 [CrossRef Medline](#)
30. Kobayashi, T., and Ikeda, K. (2006) G protein-activated inwardly rectifying potassium channels as potential therapeutic targets. *Curr. Pharm. Des.* **12**, 4513–4523 [CrossRef Medline](#)
31. Jelacic, T. M., Kennedy, M. E., Wickman, K., and Clapham, D. E. (2000) Functional and biochemical evidence for G-protein-gated inwardly rectifying K<sup>+</sup> (GIRK) channels composed of GIRK2 and GIRK3. *J. Biol. Chem.* **275**, 36211–36216 [CrossRef Medline](#)
32. Krapivinsky, G., Gordon, E. A., Wickman, K., Velimirović, B., Krapivinsky, L., and Clapham, D. E. (1995) The G-protein-gated atrial K<sup>+</sup> channel IKACH is a heteromultimer of two inwardly rectifying K<sup>+</sup>-channel proteins. *Nature* **374**, 135–141 [CrossRef Medline](#)
33. Liao, Y. J., Jan, Y. N., and Jan, L. Y. (1996) Heteromultimerization of G-protein-gated inwardly rectifying K<sup>+</sup> channel proteins GIRK1 and GIRK2 and their altered expression in weaver brain. *J. Neurosci.* **16**, 7137–7150 [CrossRef Medline](#)
34. Luján, R., and Aguado, C. (2015) Localization and targeting of GIRK channels in mammalian central neurons. *Int. Rev. Neurobiol.* **123**, 161–200 [CrossRef Medline](#)
35. Ma, D., Zerangue, N., Raab-Graham, K., Fried, S. R., Jan, Y. N., and Jan, L. Y. (2002) Diverse trafficking patterns due to multiple traffic motifs in G protein-activated inwardly rectifying potassium channels from brain and heart. *Neuron* **33**, 715–729 [CrossRef Medline](#)
36. Mirshahi, T., and Logothetis, D. E. (2002) GIRK channel trafficking: different paths for different family members. *Mol. Interv.* **2**, 289–291 [CrossRef Medline](#)
37. Chan, K. W., Langan, M. N., Sui, J. L., Kozak, J. A., Pabon, A., Ladias, J. A., and Logothetis, D. E. (1996) A recombinant inwardly rectifying potassium channel coupled to GTP-binding proteins. *J. Gen. Physiol.* **107**, 381–397 [CrossRef Medline](#)
38. Chan, K. W., Sui, J. L., Vivaudou, M., and Logothetis, D. E. (1996) Control of channel activity through a unique amino acid residue of a G protein-gated inwardly rectifying K<sup>+</sup> channel subunit. *Proc. Natl. Acad. Sci. U.S.A.* **93**, 14193–14198 [CrossRef Medline](#)
39. Slesinger, P. A., Reuveny, E., Jan, Y. N., and Jan, L. Y. (1995) Identification of structural elements involved in G protein gating of the GIRK1 potassium channel. *Neuron* **15**, 1145–1156 [CrossRef Medline](#)
40. Wydeven, N., Young, D., Mirkovic, K., and Wickman, K. (2012) Structural elements in the Girkl subunit that potentiate G protein-gated potassium channel activity. *Proc. Natl. Acad. Sci. U.S.A.* **109**, 21492–21497 [CrossRef Medline](#)
41. Chan, K. W., Sui, J. L., Vivaudou, M., and Logothetis, D. E. (1997) Specific regions of heteromeric subunits involved in enhancement of G protein-gated K<sup>+</sup> channel activity. *J. Biol. Chem.* **272**, 6548–6555 [CrossRef Medline](#)
42. Mase, Y., Yokogawa, M., Osawa, M., and Shimada, I. (2012) Structural basis for modulation of gating property of G protein-gated inwardly rectifying potassium ion channel (GIRK) by i/o-family G protein  $\alpha$  subunit (G $\alpha_{i/o}$ ). *J. Biol. Chem.* **287**, 19537–19549 [CrossRef Medline](#)
43. Days, E., Kaufmann, K., Romaine, I., Niswender, C., Lewis, M., Utley, T., Du, Y., Sliwoski, G., Morrison, R., Dawson, E. S., Engers, J. L., Denton, J., Daniels, J. S., Sulikowski, G. A., Lindsley, C. W., and Weaver, C. D. (2010) *Probe Reports from the NIH Molecular Libraries Program*, National Center for Biotechnology Information, Bethesda, MD
44. Kaufmann, K., Romaine, I., Days, E., Pascual, C., Malik, A., Yang, L., Zou, B., Du, Y., Sliwoski, G., Morrison, R. D., Denton, J., Niswender, C. M., Daniels, J. S., Sulikowski, G. A., Xie, X. S., Lindsley, C. W., and Weaver, C. D. (2013) ML297 (VU0456810), the first potent and selective activator of the GIRK potassium channel, displays antiepileptic properties in mice. *ACS Chem. Neurosci.* **4**, 1278–1286 [CrossRef Medline](#)
45. Wen, W., Wu, W., Weaver, C. D., and Lindsley, C. W. (2014) Discovery of potent and selective GIRK1/2 modulators via “molecular switches” within a series of 1-(3-cyclopropyl-1-phenyl-1H-pyrazol-5-yl)ureas. *Bioorg. Med. Chem. Lett.* **24**, 5102–5106 [CrossRef Medline](#)
46. Wieting, J. M., Vadukoot, A. K., Sharma, S., Abney, K. K., Bridges, T. M., Daniels, J. S., Morrison, R. D., Wickman, K., Weaver, C. D., and Hopkins, C. R. (2017) Discovery and characterization of 1H-pyrazol-5-yl-2-phenylacetamides as novel, non-urea-containing GIRK1/2 potassium channel activators. *ACS Chem. Neurosci.* **8**, 1873–1879 [CrossRef Medline](#)
47. Wydeven, N., Marron Fernandez de Velasco, E., Du, Y., Benneyworth, M. A., Hearing, M. C., Fischer, R. A., Thomas, M. J., Weaver, C. D., and Wickman, K. (2014) Mechanisms underlying the activation of G-protein-gated inwardly rectifying K<sup>+</sup> (GIRK) channels by the novel anxiolytic drug, ML297. *Proc. Natl. Acad. Sci. U.S.A.* **111**, 10755–10760 [CrossRef Medline](#)
48. Hunter, C. A., and Sanders, J. K. M. (1990) The nature of  $\pi$ - $\pi$  interactions. *J. Am. Chem. Soc.* **112**, 5525–5534 [CrossRef](#)
49. McGaughey, G. B., Gagné, M., and Rappé, A. K. (1998)  $\pi$ -Stacking interactions. Alive and well in proteins. *J. Biol. Chem.* **273**, 15458–15463 [CrossRef Medline](#)
50. Sun, S., and Bernstein, E. R. (1996) Aromatic van der Waals clusters: structure and nonrigidity. *J. Phys. Chem.* **100**, 13348–13366 [CrossRef](#)
51. Idevall-Hagren, O., Dickson, E. J., Hille, B., Toomre, D. K., and De Camilli, P. (2012) Optogenetic control of phosphoinositide metabolism. *Proc. Natl. Acad. Sci. U.S.A.* **109**, E2316–E2323 [CrossRef Medline](#)
52. Takemoto, Y., Slough, D. P., Meinke, G., Katnik, C., Graziano, Z. A., Chidipi, B., Reiser, M., Alhadidy, M. M., Ramirez, R., Salvador-Montañés, O., Ennis, S., Guerrero-Serna, G., Haburcak, M., Diehl, C., Cuevas, J., et al. (2018) Structural basis for the antiarrhythmic blockade of a potassium channel with a small molecule. *FASEB J.* **32**, 1778–1793 [CrossRef Medline](#)
53. Zarzoso, M., Rysevaite, K., Milstein, M. L., Calvo, C. J., Kean, A. C., Atienza, F., Pauza, D. H., Jalife, J., and Noujaim, S. F. (2013) Nerves projecting from the intrinsic cardiac ganglia of the pulmonary veins modulate sinoatrial node pacemaker function. *Cardiovasc. Res.* **99**, 566–575 [CrossRef Medline](#)
54. Johnson, P. L., Molosh, A., Fitz, S. D., Arendt, D., Deehan, G. A., Federici, L. M., Bernabe, C., Engleman, E. A., Rodd, Z. A., Lowry, C. A., and Shekhar, A. (2015) Pharmacological depletion of serotonin in the basolateral amygdala complex reduces anxiety and disrupts fear conditioning. *Pharmacol. Biochem. Behav.* **138**, 174–179 [CrossRef Medline](#)
55. Mahan, A. L., and Ressler, K. J. (2012) Fear conditioning, synaptic plasticity and the amygdala: implications for posttraumatic stress disorder. *Trends Neurosci.* **35**, 24–35 [CrossRef Medline](#)
56. Karschin, C., Dissmann, E., Stühmer, W., and Karschin, A. (1996) IRK(1–3) and GIRK(1–4) inwardly rectifying K<sup>+</sup> channel mRNAs are



## A GIRK-specific activator in conditioned fear extinction

- differentially expressed in the adult rat brain. *J. Neurosci.* **16**, 3559–3570 [CrossRef Medline](#)
57. Davis, M., and Whalen, P. J. (2001) The amygdala: vigilance and emotion. *Mol. Psychiatry* **6**, 13–34 [CrossRef Medline](#)
58. Fanselow, M. S., and LeDoux, J. E. (1999) Why we think plasticity underlying Pavlovian fear conditioning occurs in the basolateral amygdala. *Neuron* **23**, 229–232 [CrossRef Medline](#)
59. LeDoux, J. E. (2000) Emotion circuits in the brain. *Annu. Rev. Neurosci.* **23**, 155–184 [CrossRef Medline](#)
60. Lee, Y., Fitz, S., Johnson, P. L., and Shekhar, A. (2008) Repeated stimulation of CRF receptors in the BNST of rats selectively induces social but not panic-like anxiety. *Neuropsychopharmacology* **33**, 2586–2594 [CrossRef Medline](#)
61. Li, L. P., Dustrude, E. T., Haulcomb, M. M., Abreu, A. R., Fitz, S. D., Johnson, P. L., Thakur, G. A., Molosh, A. I., Lai, Y., and Shekhar, A. (2018) PSD95 and nNOS interaction as a novel molecular target to modulate conditioned fear: relevance to PTSD. *Transl. Psychiatry* **8**, 155 [CrossRef Medline](#)
62. Maren, S. (2001) Neurobiology of Pavlovian fear conditioning. *Annu. Rev. Neurosci.* **24**, 897–931 [CrossRef Medline](#)
63. Molosh, A. I., Johnson, P. L., Spence, J. P., Arendt, D., Federici, L. M., Bernabe, C., Janasik, S. P., Segu, Z. M., Khanna, R., Goswami, C., Zhu, W., Park, S. J., Li, L., Mechref, Y. S., Clapp, D. W., and Shekhar, A. (2014) Social learning and amygdala disruptions in Nf1 mice are rescued by blocking p21-activated kinase. *Nat. Neurosci.* **17**, 1583–1590 [CrossRef Medline](#)
64. Quirk, G. J., and Mueller, D. (2008) Neural mechanisms of extinction learning and retrieval. *Neuropsychopharmacology* **33**, 56–72 [CrossRef Medline](#)
65. Rogan, M. T., Stäubli, U. V., and LeDoux, J. E. (1997) Fear conditioning induces associative long-term potentiation in the amygdala. *Nature* **390**, 604–607 [CrossRef Medline](#)
66. Sosulina, L., Schwesig, G., Seifert, G., and Pape, H. C. (2008) Neuropeptide Y activates a G-protein-coupled inwardly rectifying potassium current and dampens excitability in the lateral amygdala. *Mol. Cell. Neurosci.* **39**, 491–498 [CrossRef Medline](#)
67. Manteghi, A. A., Hebrani, P., Mortezaian, M., Haghghi, M. B., and Javanbakht, A. (2014) Baclofen add-on to citalopram in treatment of posttraumatic stress disorder. *J. Clin. Psychopharmacol.* **34**, 240–243 [CrossRef Medline](#)
68. Liman, E. R., Tytgat, J., and Hess, P. (1992) Subunit stoichiometry of a mammalian  $K^+$  channel determined by construction of multimeric cDNAs. *Neuron* **9**, 861–871 [CrossRef Medline](#)
69. Jespersen, T., Grønnet, M., Angelo, K., Klærke, D. A., and Olesen, S. P. (2002) Dual-function vector for protein expression in both mammalian cells and *Xenopus laevis* oocytes. *BioTechniques* **32**, 536–538, 540 [CrossRef Medline](#)
70. Schüttelkopf, A. W., and van Aalten, D. M. (2004) PRODRG: a tool for high-throughput crystallography of protein-ligand complexes. *Acta Crystallogr. D Biol. Crystallogr.* **60**, 1355–1363 [CrossRef Medline](#)
71. Xu, Y., Wang, Y., Zhang, M., Jiang, M., Rosenhouse-Dantsker, A., Wassenaar, T., and Tseng, G. N. (2015) Probing binding sites and mechanisms of action of an I(Ks) activator by computations and experiments. *Biophys. J.* **108**, 62–75 [CrossRef Medline](#)
72. Ha, J., Xu, Y., Kawano, T., Hendon, T., Baki, L., Garai, S., Papapetropoulos, A., Thakur, G. A., Plant, L. D., and Logothetis, D. E. (2018) Hydrogen sulfide inhibits Kir2 and Kir3 channels by decreasing sensitivity to the phospholipid phosphatidylinositol 4,5-bisphosphate (PIP<sub>2</sub>). *J. Biol. Chem.* **293**, 3546–3561 [CrossRef Medline](#)
73. Lin, F. Y., and MacKerell A. D., Jr. (2017) Do halogen–hydrogen bond donor interactions dominate the favorable contribution of halogens to ligand–protein binding? *J. Phys. Chem. B* **121**, 6813–6821 [CrossRef Medline](#)
74. Scholfield, M. R., Ford, M. C., Carlsson, A. C., Butta, H., Mehl, R. A., and Ho, P. S. (2017) Structure–energy relationships of halogen bonds in proteins. *Biochemistry* **56**, 2794–2802 [CrossRef Medline](#)
75. Besler, B. H., Merz, K. M., Jr., and Kollman, P. A. (1990) Atomic charges derived from semiempirical methods. *J. Comp. Chem.* **11**, 431–439 [CrossRef](#)
76. Hickey, A. L., and Rowley, C. N. (2014) Benchmarking quantum chemical methods for the calculation of molecular dipole moments and polarizabilities. *J. Phys. Chem. A* **118**, 3678–3687 [CrossRef Medline](#)
77. Schrödinger, LLC (2019) Schrödinger Release: Induced Fit Docking Protocol; Glide. Schrödinger, LLC, New York
78. Farid, R., Day, T., Friesner, R. A., and Pearlstein, R. A. (2006) New insights about HERG blockade obtained from protein modeling, potential energy mapping, and docking studies. *Bioorg. Med. Chem.* **14**, 3160–3173 [CrossRef Medline](#)
79. Sherman, W., Day, T., Jacobson, M. P., Friesner, R. A., and Farid, R. (2006) Novel procedure for modeling ligand/receptor induced fit effects. *J. Med. Chem.* **49**, 534–553 [CrossRef Medline](#)
80. Sherman, W., Beard, H. S., and Farid, R. (2006) Use of an induced fit receptor structure in virtual screening. *Chem. Biol. Drug Des.* **67**, 83–84 [CrossRef Medline](#)